Title page

Dynamics and Regulatory Roles of RNA m^{6}A Methylation in Unbalanced Genomes

Shuai Zhang,[1,2,†] Xinyu Liu,[1,2,†] Ruixue Wang,[1,2,†] Junhan Wang,[1,2] Ludan Zhang,[1,2] and Lin Sun[1,2,*]

[1] Beijing Key Laboratory of Gene Resource and Molecular Development, College of Life Sciences, Beijing Normal University, Beijing 100875, China

[2] Key Laboratory of Cell Proliferation and Regulation Biology of Ministry of Education, College of Life Sciences, Beijing Normal University, Beijing 100875, China

† These authors contributed equally to this work.

* For correspondence: sunlin@bnu.edu.cn (Lin Sun)

Abstract

N^6-methyladenosine (m^{6}A) in eukaryotic RNA is an epigenetic modification that is critical for RNA metabolism, gene expression regulation, and the development of organisms. Aberrant expression of m^{6}A components appears in a variety of human diseases. RNA m^{6}A modification in *Drosophila* has proven to be involved in sex determination regulated by *Sxl* and may affect X chromosome expression through the MSL complex. The dosage-related effects under the condition of genomic imbalance (i.e., aneuploidy) are related to various epigenetic regulatory mechanisms. Here, we investigated the roles of RNA m^{6}A modification in unbalanced genomes using aneuploid *Drosophila*. The results showed that the expression of m^{6}A components changed significantly under genomic imbalance, and affected the abundance and genome-wide distribution of m^{6}A, which may be related to the developmental abnormalities of aneuploids. The relationships between methylation status and classical dosage effect, dosage compensation, and inverse dosage effect were also studied. In addition, we demonstrated that RNA m^{6}A methylation may affect dosage-dependent gene regulation through dosage-sensitive modifiers, alternative splicing,

the MSL complex, and other processes. More interestingly, there seems to be a closely relationship between MSL complex and RNA m^{6}A modification. It is found that ectopically overexpressed MSL complex, especially the levels of H4K16Ac through MOF could influence the expression levels of m^{6}A modification and genomic imbalance may be involved in this interaction. We found that m^{6}A could affect the levels of H4K16Ac through MOF, a component of the MSL complex, and that genomic imbalance may be involved in this interaction. Altogether, our work reveals the dynamic and regulatory role of RNA m^{6}A modification in unbalanced genomes, and may shed new light on the mechanisms of aneuploidy-related developmental abnormalities and diseases.

Introduction

Epigenetic modifications regulate gene expression in response to environmental changes and play important roles in the development of organisms and a variety of human diseases (Jaenisch and Bird, 2003; Lence et al., 2017). In addition to DNA and chromatin modifications, which are well studied, more than one hundred RNA chemical modifications have been identified in cells to date (Lee et al., 2014; Roundtree et al., 2017a). As a marker of post-transcriptional regulation, RNA modifications participate in almost all aspects of RNA metabolism (Roundtree et al., 2017a). *N*^{6}-methyladenosine (m^{6}A) is the most prevalent internal modification in many eukaryotic messenger RNAs (mRNAs) and long noncoding RNAs (lncRNAs) (Lee et al., 2014; Roundtree et al., 2017a; Yang et al., 2018), which widely affects RNA alternative splicing (Dominissini et al., 2012), export (Roundtree et al., 2017b), stability (Wang X et al., 2014), and translation (Meyer et al., 2015). RNA m^{6}A modifications have been found to be enriched on the transcripts of genes that regulate development and cell fate specification (Dominissini et al., 2012; Meyer et al., 2012; Geula et al., 2015), and some m^{6}A sites are regulated in a tissue- or disease-specific manner (Zaccara et al., 2019). In addition, the abnormal expression of m^{6}A components is related to the tumorigenesis, proliferation, and metastasis of many types of cancers (Pinello et al., 2018; Ma et al., 2019). Therefore, it is of great significance to study RNA m^{6}A methylation for revealing the mechanisms of gene expression regulation and human diseases.

57 At present, there are few studies on RNA m^6A modification in *Drosophila*, possibly due to its
58 relatively low abundance ($m^6A/A < 0.2\%$) (Haussmann et al., 2016), and the mutation of some
59 m^6A component genes will affect their viability and fertility (Hongay and Orr-Weaver, 2011;
60 Haussmann et al., 2016; Kan et al., 2017). However, as a model organism with specific genetic
61 and developmental advantages, *Drosophila* remains an excellent tool for studying the roles of
62 epigenetic modifications in gene regulation, individual development, and disease process. Several
63 components of the *Drosophila* m^6A methyltransferase complex (*Ime4*, *dMettl14*, and *fl(2)d*
64 constitute the core complex, with *vir* and *nito* acting as cofactors) and a m^6A reader protein
65 (*Ythdc1*) have been identified, all of which have homologues in mammals (Lence et al., 2017).
66 Deletion of the major methyltransferase gene *Ime4* or the reader *Ythdc1* causes locomotion
67 defects, and the splicing of sex-determining factor *Sxl* is affected (Haussmann et al., 2016; Lence
68 et al., 2016; Kan et al., 2017). However, homozygous mutations in *fl(2)d*, *vir*, and *nito* were lethal,
69 suggesting that these subunits have important functions other than methylation (Penn et al.,
70 2008; Yan et al., 2015; Kan et al., 2017; Lence et al., 2017). RNA m^6A modification has an obvious
71 sexual dimorphism in *Drosophila*, and reduced m^6A levels severely decreased the survival of
72 females. It is thought to be due to the derepression of *msl-2* caused by aberrantly spliced *Sxl*,
73 which forms the Male Specific Lethal (MSL) complex that associates with the X chromosome
74 (Haussmann et al., 2016).
75 Dosage compensation is a widespread phenomenon in unbalanced genomes (Lucchesi, 2018;
76 Birchler and Veitia, 2021). The deletion or duplication of some chromosomes rather than the
77 whole chromosome set leads to genomic imbalance, that is, aneuploidy (Orr et al., 2015).
78 Aneuploid variation is usually detrimental to organisms (Birchler and Veitia, 2012; Orr et al., 2015;
79 Birchler and Veitia, 2021), and is associated with developmental abnormalities, mental
80 retardation, and various congenital defects (Williams et al., 2008; Huang et al., 2021;
81 Sanchez-Pavon et al., 2021), possibly due to disorders in their gene expression systems (Prestel et
82 al., 2010; Letourneau et al., 2014). Studies across species have pointed out that there is
83 genome-wide *trans* modulation in aneuploidy, and the genes on the varied chromosomes are
84 compensated to a certain extent, while genes located on the rest of the genome are mainly
85 regulated in the opposite direction to the changes of chromosome numbers, which is known as
86 the inverse dosage effect (Birchler and Veitia, 2012, 2021; Sun et al., 2013c; Hou et al., 2018; Shi

et al., 2021). Histone modification (Zhang et al., 2021a), chromatin remodeling (Birchler, 2016), lncRNAs (Zhang et al., 2023) and microRNAs (Shi et al., 2022) have all been shown to play a role in genomic imbalance.

Because of the haploinsufficiency for X-linked genes, heterogametic individuals in organisms with XY sex determination systems could be regarded as analogous to aneuploidy (Disteche, 2016), including humans and *Drosophila*. Some studies have linked histone H4 lysine 16 acetylation (H4K16ac) and non-coding *roX* RNAs to the dosage compensation of *Drosophila* (Park et al., 2010; Conrad et al., 2012). On the other hand, the compensation of X chromosome in human is thought to be regulated by lncRNA X-inactive specific transcript (*XIST*) (Jordan et al., 2019). Interestingly, in *Drosophila*, RNA m^6A modification indirectly affects gene expression through *Sxl* and *msl-2*; while in human, m^6A methylation of the key lncRNA *XIST* is necessary for the silencing of gene transcription on one of the female X chromosomes (Patil et al., 2016). Moreover, most tumor cells have genomic instability and high levels of aneuploidy (Ben-David and Amon, 2020; Chiarle, 2021), and at the same time, m^6A component genes are often aberrantly expressed in various cancers (Pinello et al., 2018; Ma et al., 2019).

An increasing number of studies have found that dosage-related effects in aneuploidy may be the integration of multiple modulations rather than through a single mechanism (Prestel et al., 2010; Birchler, 2016). The effects of genomic imbalance are complicated, and the model of dosage compensation and global gene regulation in *Drosophila* has been extended to autosomal aneuploidies and sex chromosome aneuploid metafemales where MSL complexes are not assembled (Sun et al., 2013b,c; Zhang et al., 2021b). In addition, genomic imbalance and *trans* regulatory mechanisms in other species such as maize, *Arabidopsis*, and humans have also been investigated (Hou et al., 2018; Raznahan et al., 2018; Shi et al., 2021; Yang et al., 2021; San Roman et al., 2023). To reveal the role of RNA m^6A modification in unbalanced genomes, we studied the dynamic changes and regulatory functions of m^6A methylation under genetic imbalance conditions using autosomal and sex chromosome aneuploid *Drosophila* maintained in our laboratory. Meanwhile, dosage-sensitive modifiers, differential alternative splicing events, the MSL complex and other factors that may mediate the relationships between RNA m^6A modification and the dosage-related effects of aneuploidy were also investigated. In summary, we provided a comprehensive picture of RNA m^6A methylation in unbalanced genomes.

117

118

119 ## Results

120 ### The responses of m^{6}A components under genomic imbalance

121 RNA m^{6}A methylation is a reversible epigenetic modification, and its dynamic process is mediated
122 by m^{6}A methyltransferases (writers), demethylases (erasers), and m^{6}A recognition proteins
123 (readers) (Lee et al., 2014; Yang et al., 2018; Zaccara et al., 2019) (Figure 1A). We first detected
124 the expression of m^{6}A components in *Drosophila* larvae with karyotypes of normal diploids and
125 trisomies that have an additional chromosome arm using RT-qPCR to determine whether RNA
126 m^{6}A dynamics are affected by correlative enzymes in unbalanced genomes (Figure 1B; Figure
127 1—figure supplement 1A,B). It was found that the transcription levels of most m^{6}A writers and
128 the major m^{6}A reader are down-regulated in aneuploids compared with their respective
129 sex-corresponding controls (Figure 1B). Unlike the other components, the cofactor *vir* of
130 methyltransferase complex is up-regulated in trisomy 2L females (Haussmann et al., 2016; Lence
131 et al., 2016; Kan et al., 2017). Because RNA m^{6}A modification is enriched in the nervous system of
132 *Drosophila*, the brains of aneuploid third instar larvae were also used to detect the expression of
133 m^{6}A components. As expected, a decreased expression trend of m^{6}A components similar to that
134 of the whole larvae was observed (Figure 1—figure supplement 1C).

135 Previous studies have pointed out that the m^{6}A methylomes have temporal and spatial
136 specificity in the development process of organisms, especially for embryonic development and
137 cell differentiation (Meyer and Jaffrey, 2014; Wang Y et al., 2014). Aberrant expression of m^{6}A
138 components may cause defects in embryogenesis and even early embryonic lethality (Zhong et
139 al., 2008; Wang Y et al., 2014; Geula et al., 2015; Zhao et al., 2017). Therefore, we designed
140 probes of m^{6}A components (Figure 1—figure supplement 1D,E) to examine the mRNA expression
141 and localization patterns during early embryonic development of aneuploid *Drosophila* using
142 high-resolution TSA-FISH (Lecuyer et al., 2007; Jandura et al., 2017). The results showed that the
143 subembryonic distribution patterns of the five components of m^{6}A methyltransferase complex
144 and one m^{6}A reading protein are similar in wildtype and aneuploidies (Figure 1C,D; Figure

145 1—figure supplement 2A-F). At the blastoderm stage (stage 1-5), the probe signals of m^{6}A
146 components are widely distributed in the surface cell layer, yolk plasma, yolk cortex, and show a
147 pattern of basal enrichment (Figure 1—figure supplement 2A-F). For the gastrulae at stage 6-11,
148 the transcripts of m^{6}A components are mainly located in head, amnioproctodeal invagination,
149 germ band, and as in previous studies (Lence et al., 2016), and show an enrichment in
150 neuroectoderm (Figure 1C; Figure 1—figure supplement 2A-F). At later stages of embryonic
151 development (stages 12-13 and 14-17), the probes are distributed in brain, ventral nerve cord,
152 midgut, and salivary gland (Figure 1C; Figure 1—figure supplement 2A-F).

153 By observing the subcellular localization of the probe signals of m^{6}A components at higher
154 magnification, it can be found that most of the mRNAs of these genes have nuclei-associated
155 localization patterns (Figure 1D; Figure 1—figure supplement 2A'-F'). In the early and late stages
156 of embryonic development, the probe signals of *Ime4*, *dMettl14*, *fl(2)d*, *vir*, and *Ythdc1* form
157 dense small foci near the nucleus, which is a perinuclear distribution (Figure 1D; Figure 1—figure
158 supplement 2A'-F'). For *nito*, in addition to the perinuclear signals, there is also an obvious signal
159 of intranuclear localization during early embryogenesis, which is manifested as one or two small
160 foci in the blastoderm nucleus (Figure 1D; Figure 1—figure supplement 2E').

161 Although there seems to be no difference in the localization of the transcripts of m^{6}A
162 components that we detected in aneuploidy and wildtype embryos, the expression levels of
163 these genes, as determined by relative fluorescence intensity, are significantly changed (Figure
164 1E,F; Figure 1—figure supplement 2A"-F"). Except for the irregular fluctuations at early
165 embryonic stages, the expression levels of most m^{6}A components in aneuploids are lower than
166 those in wildtype at more mature stages (Figure 1E,F; Figure 1—figure supplement 2A"-F"), which
167 is similar to the trend we detected in third instar larvae (Figure 1B; Figure 1—figure supplement
168 1C). The transcripts of m^{6}A methyltransferase and reader protein have specific subembryonic and
169 subcellular localization patterns in the development of *Drosophila* embryos, which may be a
170 mechanism to regulate cellular functions, and ensure appropriate cell growth and differentiation
171 (Lecuyer et al., 2007).

172

173 **Genome-wide mapping of RNA m^{6}A methylation in aneuploid *Drosophila***

174 Subsequently, we detected the global levels of RNA m^6A methylation in wildtype and aneuploid
175 *Drosophila* larvae to determine whether m^6A abundance is altered under the condition of
176 genomic imbalance due to modulation by transmethylases. The overall abundance of m6A was
177 represented by the m^6A/A ratio in total RNA (Figure 2A). It was found that the m^6A abundance of
178 wildtype males is higher than that of females, but both are lower than 0.2%, which is consistent
179 with the finding that m^6A levels in *Drosophila* are relatively low (Haussmann et al., 2016; Lence et
180 al., 2016). Females with triple chromosome 2 left arms (2L) and metafemales with triple X
181 chromosomes have significantly higher m^6A abundances than diploid females, whereas there is
182 no significant difference between trisomy 2L males and wildtype males (Figure 2A). Therefore,
183 genomic imbalance can affect the m^6A methylation status to some extent, and this epigenetic
184 modification is different between males and females. However, the m^6A abundance in
185 aneuploidies did not follow the expression levels of transmethylases.

186 To obtain m^6A mapping across the transcriptome of aneuploid *Drosophila*, samples with
187 different karyotypes were used for m^6A methylated RNA immunoprecipitation sequencing
188 (MeRIP-Seq). By identifying consistent peaks in two biological replicates, approximately ten
189 thousand m^6A peaks were found in wildtype females and males, whereas there were less than
190 half the number of methylation sites in the three kinds of aneuploidies (Figure 2B). When these
191 m^6A sites were annotated according to the nearest genes, the changes in the number of
192 m^6A-marked genes in samples of different genotypes were in accordance with that of m^6A peaks,
193 in which there are about 2,500 m^6A-marked genes in wildtype and about 1,000 m^6A-modified
194 genes in trisomies (Figure 2C). Both the number of m^6A peaks and the number of m^6A-modified
195 genes are the least in trisomy 2L females (Figure 2B,C). The changes in the number of RNA
196 methylation sites in aneuploids did not coincide with the changes of overall m^6A abundance, but
197 instead matched the expression of m^6A components. We speculate that this may be caused by
198 the nonuniformity and heterogeneity of RNA m^6A modification, including the tissue specificity,
199 the developmental specificity, the different numbers of m^6A sites in one transcript, the different
200 proportions of methylated transcripts, et cetera (Meyer et al., 2012; Meyer and Jaffrey, 2014;
201 Zaccara et al., 2019). Analysis of m^6A-modified reads in wildtype and aneuploidy MeRIP samples
202 showed that the expression levels at m^6A sites in aneuploidies are significantly higher than that in
203 wildtype (Mann Whitney U test p-values < 0.001; Figure 2D), which confirmed our hypothesis.

204 These results suggest that RNA m^6A modification exhibits greater heterogeneity in unbalanced
205 genomes.

206 We next studied the overall characteristics of m^6A methylation in aneuploid and control
207 *Drosophila*. m^6A peaks are localized along all autosomes and sex chromosomes, and the numbers
208 of peaks are correlated with chromosome length (Figure 2—figure supplement 1A). Methylation
209 sites are widely distributed on 5'UTR (30-50%), 3'UTR (10-15%), promoter (15-20%), and internal
210 exons (20-35%), and the aneuploidies appeared to have a higher proportion of 5'UTR peaks and a
211 lower proportion of exon peaks than the wildtype (Figure 2E). The highest values of density
212 distributions of the length of exons containing m^6A peaks are around 250 bp, and approximately
213 90% of the exons are longer than the typical 140 bp (Figure 2—figure supplement 1B). *De novo*
214 motif analysis of m^6A methylation peaks in each sample showed that the top-ranked motif is
215 consistent with the conserved m^6A motif DRACH (D=G/A/U, R=G/A, H=U/A/C; Figure 2F). In
216 addition, enrichment analysis of the known motif DRACH showed that it is significantly enriched
217 in all samples, and more than 97% of the m^6A sites have this sequence (Figure 2—figure
218 supplement 1C).

219 There are 370 common genes to which the m^6A peaks were annotated in all genotypes
220 (Figure 2G). We classified the m^6A-modified genes in each sample and found that they were
221 mostly protein-coding genes, whereas only about 7% were ncRNAs (Figure 2H). As described in
222 previous studies (Meyer et al., 2012; Zaccara et al., 2019), most methylated RNAs have one m^6A
223 peak (Figure 2—figure supplement 1D-H). However, there are still some genes whose transcripts
224 can be highly methylated and contain more than five m^6A sites (Figure 2—figure supplement
225 1D-I). It was found that transcription factors were significantly enriched in 70 genes with more
226 than 5 m^6A peaks in both wildtype and aneuploidy (Fisher's exact test p-value = 7.7e-4; Figure 2I;
227 Figure 2—figure supplement 1I). Thus, specific types of genes may be preferentially targeted by
228 m^6A modification, such as transcriptional regulators (Kan et al., 2017). Analysis of the functions of
229 m^6A-modified genes in each sample revealed that they were enriched for a large number of
230 common functions, among which the most significant were those related to morphogenesis,
231 development, and growth (Figure 2—figure supplement 2A). The 141 GO terms shared by the
232 five genotypes were summarized and found to include functions about metabolism, regulation,
233 cellular processes, signaling pathways, behavior, and immune response (Figure 2—figure

234 supplement 2B,C). Through pathway enrichment analysis of m^6A-modified genes, 9 terms were
235 found to be consistently enriched in all samples, including MAPK signaling pathway, Hippo
236 signaling pathway, TGF-β pathway, etc. (Figure 2—figure supplement 2D-F).
237

238 **Differentially methylated peaks (DMPs) and their associated genes**

239 We then searched for the differential methylation peaks (DMPs) in autosomal and sex
240 chromosome aneuploidies compared with wildtype *Drosophila* of their corresponding sex. The
241 number of DMPs and the changing trend of DMP methylation status are shown in the Figures
242 (Figure 3A-D). In trisomy 2L females, the number of upregulated DMPs (1,131) is less than that of
243 downregulated DMPs (1,602). In trisomy 2L males, the number of upregulated DMPs (1,521) is
244 slightly higher than that of downregulated DMPs (1,259). In metafemales, the number of
245 upregulated DMPs (1,393) is higher than that of downregulated DMPs (926) (Figure 3A-D). More
246 DMP-associated genes were found in autosomal aneuploidies than in sex chromosome
247 aneuploidy (trisomy 2L female = 2,148, trisomy 2L male = 2,055, metafemale = 1,771; Figure 3E).
248 Also, the total number of peaks after the differential analysis would be different from the number
249 of m^6A peaks identified in the previous section, because the analysis software merged and
250 recalculated the peaks (Stark and Brown, 2013).

251 DMPs are distributed on all chromosomes (Figure 3—figure supplement 1A). Specifically, the
252 MeRIP-Seq signal intensity at the location of DMPs showed that the m^6A-marked reads in
253 trisomies are denser than those of wildtypes, especially on the triple chromosomes (Figure 3F-H).
254 The density of reads on chromosome 2L of trisomy 2L *Drosophila* is higher than that on other
255 chromosomes, while the density of reads on chromosome X of metafemales is significantly higher
256 than that of autosomes (Figure 3F-H). Previous studies on aneuploid *Drosophila* showed that the
257 expression levels of genes on chromosomes with increased copy numbers were mostly similar to
258 those in diploids, and the expression of genes on unvaried chromosomes were widely inverse
259 regulated (Sun et al., 2013c; Birchler, 2016; Zhang et al., 2023). It can be concluded that the
260 changes in the density of reads at DMP sites are not due to a direct gene dosage effect. Similar
261 results were obtained by counting the methylation status of cis and trans transcripts (Figure 3I-K).
262 Overall, the transcripts of genes located on the varied chromosomes in three trisomies have

263 more up-regulated DMPs than down-regulated DMPs, which is more obvious in metafemales
264 (Figure 3I-K). In trisomy 2L females and males, genes localized on other autosomes have a higher
265 proportion of down-regulated DMPs, while the X-linked *trans* genes show sexual dimorphism and
266 X chromosome-specific response to genomic imbalance. (Figure 3I,J). For metafemales, the
267 transcripts of *trans* genes have similar numbers of up-regulated and down-regulated DMPs
268 (Figure 3K). Therefore, *cis* genes in trisomy generally possessed a higher proportion of
269 up-regulated DMP-associated transcripts, whereas the methylation states of *trans* genes are
270 variable, depending on the identities of varied chromosomes and their genomic locations. The
271 above results give us reason to speculate that the changes of m^6A methylation may affect dosage
272 compensation of *cis*-genes and inverse dosage modulation of *trans*-genes in aneuploidy.

273 The distribution of DMPs along gene features includes 5'UTR (30-35%), 3'UTR (20-25%),
274 promoter (10-25%), and internal exon (25-35%), among which the proportion of 3'UTR is higher
275 than that of all m^6A sites (Figure 3—figure supplement 1B). The length distributions of exons with
276 DMPs are similar to that of all m^6A-modified exons (Figure 3—figure supplement 1C). *De novo*
277 motif analysis of the sequences where DMPs are located or enrichment analysis of the known
278 motif DRACH both showed that DMP sites are enriched for the conserved motif of m^6A (Figure
279 3—figure supplement 1D,E). There are also similarities between the types of DMPs-associated
280 genes and m^6A-marked genes (Figure 3—figure supplement 1F). The DMP-associated genes of
281 the three aneuploidies have complex overlapping relationships (Figure 3—figure supplement 1G).
282 Most DMP-associated genes have one differentially methylated site, and only a few genes
283 contained more than three DMPs (Figure 3—figure supplement 1H-J). There are 1,042 common
284 DMP-associated genes in all trisomies, of which 71 were transcription factors and were
285 significantly enriched (Fisher's exact test p-value = 6.9e-5; Figure 4A,B). We speculate that these
286 differentially methylated transcription factors may play an important role in the regulation of
287 gene expression and development of aneuploidy.

288 Functional enrichment analysis showed that genes with up-regulated DMPs in three trisomies
289 were enriched for 153 common functions, while the genes with down-regulated DMPs shared
290 only 6 functions (Figure 4—figure supplement 1A,B). Similarly, genes with up-regulated DMPs
291 were enriched for more consistent pathways in all aneuploids (Figure 4—figure supplement 1C,D).
292 Most of the functions of DMP-associated genes are the same as those of m^6A-marked genes, and

293 these genes are also enriched for cell fate commitment, dorsal/ventral pattern formation, sex
294 differentiation, post-transcriptional regulation of gene expression, and other additional GO terms.
295 We found that many DMP-associated genes have functions related to gene expression regulation
296 and dosage compensation, including some components of MSL complex (*msl-1*, *msl-3*,
297 *lncRNA:roX1*) and the major sex-determining factor *Sxl* (Figure 4C). We also noticed that m^6A
298 component genes *fl(2)d*, *nito*, and *Ythdc1* themselves are differentially methylated in aneuploidy
299 (Figure 4C), for example, there was a common significantly upregulated m^6A peak in the 5'UTR of
300 the transcripts of *fl(2)d* in three aneuploidies (Figure 4D). These data suggest that m^6A dynamics
301 in aneuploids may be involved in the expression regulation of unbalanced genomes through
302 various genes with regulatory functions.
303

304 Relationships between m^6A and dosage-related modulation of gene expression in 305 aneuploidy

306 To explore the relationships between RNA m^6A modification and gene expression regulation
307 under genomic imbalance, we combined the results of MeRIP-Seq and RNA-seq, and performed a
308 comprehensive analysis. The results showed that about 12%-15% of genes differentially
309 expressed in aneuploid *Drosophila* also belong to DMPs-associated genes (Figure 5A-C). However,
310 except for trisomy 2L males, the DEGs of the other two trisomies did not show enrichment of
311 differential m^6A methylation (Fisher's exact test p-values: trisomy 2L male = 0.012, trisomy 2L
312 female and metafemale > 0.05). There are 55 genes that are both differentially expressed and
313 differentially methylated in all aneuploidies (Figure 5D). By analyzing the functions of genes that
314 are simultaneously differentially expressed and differentially methylated, we obtained a number
315 of consistent biological functions, including post-embryonic animal morphogenesis, cell
316 communication, signal transduction, response to stimulation, and so on (Figure 5E), possibly
317 reflecting the important roles of m^6A-regulated expression in cell signaling and development of
318 organisms.

319 By analyzing the crossover of different groups of m^6A-modified genes and genes with
320 canonical dosage effect, dosage compensation, and inverse dosage effect, we further revealed
321 the relationships between m^6A-modified genes and dosage-related effects in aneuploidy (Figure

322 5F-H). The results showed that in trisomy 2L females, *cis* dosage compensation genes, *trans*
323 autosomal dosage effect genes, and *trans* unchanged genes are significantly enriched in m^6A
324 group with methylation in both trisomy and control; meanwhile, *cis* dosage effect genes, other
325 autosomal dosage effect genes, and X-linked dosage effect genes are enriched in the group
326 without methylation in both trisomy and control (Figure 5F). On the contrary, in trisomy 2L males,
327 *cis* dosage effect genes, *trans* dosage effect genes, and *trans* unchanged genes are significantly
328 enriched in m^6A group whose genes are methylated in both trisomy and control; while the group
329 of genes that are not methylated at all is enriched for *cis* dosage effect genes, *cis* dosage
330 compensation genes, *trans* inverse dosage effect genes, and other autosomal dosage effect genes
331 (Figure 5G). Metafemales performed similarly to trisomy 2L female, with significant enrichment
332 of *cis* dosage compensation genes, autosomal *trans* dosage effect genes, and *trans* unchanged
333 genes in m^6A group where both trisomy and control genes are methylated; and the group
334 without methylation is enriched for *cis* dosage effect genes and *trans* dosage effect genes (Figure
335 5H). These results indicated that m^6A-modified genes in aneuploid *Drosophila* females are mainly
336 related to dosage compensation and inverse dosage effect, while genes not modified by m^6A are
337 mainly related to direct dosage effect. Male aneuploids did not follow this trend.

338 Furthermore, the distributions of m^6A modification sites along gene features in genes with
339 classical dosage-related effects were also studied (Figure 5I-K). We found that in wildtype females,
340 trisomy 2L females, and metafemales, a higher proportion of m^6A sites on genes with canonical
341 dosage compensation and inverse dosage effect are distributed in the 5'UTR than genes with
342 dosage effects (Figure 5I,K). At the same time, this proportion is higher in trisomy than in
343 wildtype. In contrast to females, trisomy 2L males have a higher proportion of 5'UTR RNA m^6A
344 modification on dosage effect genes (Figure 5J). The above study again demonstrates the sexual
345 dimorphism of RNA m^6A modification in response to aneuploidy. In addition, it has been
346 suggested that m^6A residues in the 5'UTR region may have unique regulatory functions (Luo et al.,
347 2014; Meyer and Jaffrey, 2014). Therefore, we hypothesized that the high level of 5'UTR m^6A
348 modification on genes with dosage compensation and inverse dosage effect might regulate the
349 down-regulation of these genes.

350 Dozens of dosage-sensitive modifiers have been identified in *Drosophila*, whose dosage
351 changes can negatively or positively regulate the gene expression across the whole genome like

352 aneuploidy (Birchler et al., 2001; Birchler and Veitia, 2007). Protein-protein interaction (PPI)
353 networks between dosage-sensitive modifiers and differentially expressed genes (DEGs) were
354 constructed to investigate whether RNA m^6A modification could participate in the gene
355 regulatory networks in unbalanced genomes through these regulators (Figure 5—figure
356 supplement 1A-C). In the three types of aneuploidies, there are more dosage-sensitive modifiers
357 with up-regulated DMPs than with down-regulated DMPs. The regulators *ox* and *Vha55* without
358 DMPs interact with a large number of significantly up-regulated DEGs in trisomy 2L females and
359 metafemales, whereas these two regulators interact with a small number of down-regulated
360 DEGs in trisomy 2L males. Up-regulated DMP-associated regulators *wg*, *Uba1*, *ap*, *Atg1*, *osa*, *rdx*,
361 and *sd* in trisomy 2L females mainly interacted with significantly down-regulated DEGs (Figure
362 5—figure supplement 1A); and up-regulated DMP-associated regulators *Uba1*, *osa*, and *sd* in
363 metafemales also interacted with down-regulated DEGs (Figure 5—figure supplement 1C).
364 Up-regulated DMP-associated regulators *wg*, *Kr-h1*, and *Trl* mainly interacted with up-regulated
365 DEGs in trisomy 2L males (Figure 5—figure supplement 1B). In addition, a preponderance of
366 significantly down-regulated DEGs interacted with dosage-sensitive modifiers is observed on
367 *trans* chromosomes of all *Drosophila* trisomies (Figure 5—figure supplement 1A-C).
368

369 Alterations of m^6A may be involved in differential alternative splicing in imbalanced 370 genomes

371 Next, we analyzed the differential alternative splicing events in aneuploid *Drosophila*. More than
372 1,000 differential splicing events have been identified in different aneuploids, and about
373 one-third of them are of the type of skipped exon (SE) (Figure 6—figure supplement 1A-C). The
374 biological functions of differentially spliced transcripts are mainly involved in macromolecular
375 fiber organization, locomotion, and growth (Figure 6—figure supplement 1D), and these genes
376 are enriched in heterogeneous pathways in different aneuploidies (Figure 6—figure supplement
377 1E). Notably, we found that genes with DMPs are significantly enriched for differential alternative
378 splicing events in three kinds of aneuploid *Drosophila* (Fisher's exact test p-values < 0.05; Figure
379 6A-C). Among the genes whose transcripts are differentially spliced, 27%-32% are also
380 differentially methylated (Figure 6A-C). There are 67 genes with both differential alternative

381 splicing and differential m^6A methylation in all aneuploidies (Figure 6D). The functions of these
382 genes are similar to those of all differentially spliced genes (Figure 6E), but more consistent KEGG
383 pathways are enriched, including endocytosis, mTOR signaling pathway, Hedgehog signaling
384 pathway, and so on (Figure 6F).

385 In all trisomy *Drosophila*, 10 genes are shown to be differentially expressed, with their
386 transcripts also being differentially spliced and differentially methylated. Three of them are
387 illustrated below [*su(Hw)*, *Ppn*, and *CG13124*]. *su(Hw)* is a component of the gypsy chromatin
388 insulator complex, which is a regulatory element that establish independent domains of
389 transcriptional activity (Roseman et al., 1993). Due to the close relationship between *su(Hw)* and
390 second-site modifiers (Rabinow and Birchler, 1989), and *BEAF-32*, which is also an insulator
391 DNA-binding protein, has been proposed as a possible inverse dosage regulator (Gurudatta et al.,
392 2012; Zhang et al., 2021b), We speculated that the transcription factor *su(Hw)* may also be a
393 dosage-sensitive regulator. The data showed that the transcription levels of *su(Hw)* are
394 up-regulated in all three aneuploidies, and there is a consistent m^6A modification site with
395 significantly down-regulated methylation (Figure 6G). At the same time, the transcripts of this
396 gene have a common alternative 5' splice site (A5SS), and its inclusion levels in trisomies are
397 down-regulated, that is, more short transcript isoforms are generated (Figure 6G). *Ppn* gene
398 encodes an essential extracellular matrix protein that influences cell rearrangements. The
399 expression level of *Ppn* and its m^6A methylation in 5'UTR region are both significantly
400 up-regulated in trisomies (Figure 6—figure supplement 1F). In addition, an alternatively spliced
401 exon is significantly less frequently skipped in all aneuploid *Drosophila* (Figure 6—figure
402 supplement 1G). The third gene, *CG13124*, which may be involved in involved in regulation of
403 translational initiation, is up-regulated in aneuploids. Two m^6A sites in its 5'UTR region are
404 methylated at higher levels in all aneuploid *Drosophila* (Figure 6—figure supplement 1H). Its
405 transcripts also have a common significantly different exon-skipping event (Figure 6—figure
406 supplement 1I).

407 These results indicate that there are complicated relationships among RNA m^6A modification,
408 gene expression, and alternative splicing under the condition of genome imbalance. RNA splicing
409 seems to be more closely related to m^6A methylation than gene transcription. The m^6A sites
410 located in 5'UTR show remarkable changes in methylation levels in aneuploid *Drosophila*, and

411 may be involved in the regulation of some differential alternative splicing events, such as exon
412 skipping.
413

414 **Interactions between m^{6}A and *Drosophila* Male Specific Lethal (MSL) complex**

415 Previous studies have shown that m^{6}A components are involved in regulating the alternative
416 splicing of sex-determining gene *Sxl* in *Drosophila*, and the deficiency of m^{6}A writers or readers
417 will lead to the reduction of female-specific isoforms of *Sxl* (Haussmann et al., 2016; Lence et al.,
418 2016; Kan et al., 2017). *Sxl* is also a direct target of RNA m^{6}A modification (Kan et al., 2017). We
419 found that *Sxl* transcripts are both differentially methylated and differentially spliced in three
420 kinds of aneuploid *Drosophila* (Figure 7A,B). For trisomy 2L females and metafemales, two
421 common m^{6}A peaks are significantly up-regulated in the 5'UTR region of *Sxl*. However, trisomy 2L
422 males have a significantly down-regulated m^{6}A peak in the 5'UTR (Figure 7A). Meanwhile,
423 multiple junctions of *Sxl* transcripts undergo complicated alternative splicing in aneuploid
424 *Drosophila*, including SE, A5SS, alternative 3' splice site (A3SS), and mutually exclusive exons
425 (MXE) types (Figure 7A). By checking the distributions of RNA sequencing reads near the
426 male-specific exon (namely the third exon), it can be observed that there are almost no mapped
427 reads on the third exon in wildtype females, trisomy 2L females, and metafemales, while the
428 reads mapped to the second and fourth exons are highly prevalent (Figure 7B). On the contrary,
429 wildtype males and trisomy 2L males have a substantial number of reads on the third exon,
430 accompanied by a smaller number of reads on the adjacent two exons (Figure 7B). Notably, we
431 found that a small number of RNA-seq reads aligned to the male-specific exon appeared in
432 trisomy 2L females, which was identified as an SE-type differential alternative splicing event (FDR
433 = 7.4e-7; Figure 7B). This variation may be related to the abnormal m^{6}A methylation levels under
434 the condition of genomic imbalance.

435 The abnormal expression of m^{6}A components reduces the survival of female *Drosophila*,
436 which is thought to be probably caused by the expression of downstream MSL complex
437 (Haussmann et al., 2016). To investigate the interplay between the MSL complex and m^{6}A
438 modification, we examined the responses of m^{6}A regulators in transgenic *Drosophila* strains with
439 MSL2 mutation or overexpression (Figure 7—figure supplement 1A-E; Figure 7C,D). The results

440 revealed significant changes in the expression profiles of m^{6}A regulators in MSL2 transgenic
441 strains, especially the m^{6}A reader protein Ythdc1, which increased tens of fold in MSL2
442 knockdown and overexpressed *Drosophila* (Figure 7C,D; Figure 7—figure supplement 1E). We
443 also observed that the trends of Ime4 expression in females and males were the same in
444 MSL2-overexpressed *Drosophila*, whereas there was obvious sexual dimorphism in
445 MSL2-knockdown samples (Figure 7C,D), which may be due to the ectopic assembly of MSL
446 complex in MSL2-overexpressed females (Zhang et al., 2021a). In addition, we also examined the
447 expression levels of MSL2 when *Ythdc1* was knocked down, and found that MSL2 was also
448 significantly increased in females (Figure 7—figure supplement 1F). All these results strongly
449 suggest a potential relationship between MSL2 and Ythdc1. Next, we further compared the
450 overall abundance of m^{6}A in MSL2 transgenic and wildtype *Drosophila* (Figure 7E,F). The results
451 showed that m^{6}A levels were significantly decreased with MSL2 knockdown and significantly
452 increased with MSL2 overexpression in females (Figure 7E). However, overexpression of MSL2
453 failed to exert a discernible effect on m^{6}A abundance in males, although m^{6}A level decreased
454 with MSL2 depletion (Fig.7F). This difference between the sexes may be due to the endogenous
455 MSL2 in males, but not in females.

456 In the next, we investigated the expression of m^{6}A regulators in aneuploid *Drosophila*
457 overexpressing MSL2, according the results that the MSL complex could be regulated directly or
458 indirectly by m^{6}A modification, and the sexual dimorphism of RNA m^{6}A modification in response
459 to aneuploidy. It is found that the transcription levels of m^{6}A regulators are significantly
460 up-regulated in the brains of most aneuploid larvae that overexpressed MSL2 (Figure 7G; Figure
461 7—figure supplement 1G). These results are not completely consistent with the quantitative
462 results when MSL2 was overexpressed in diploids, which may be related to the effect of
463 unbalanced genomes. We also used TSA-FISH to detect the expression and distribution of m^{6}A
464 components during embryogenesis in aneuploidies overexpressing MSL2 (Figure 7H; Figure
465 1—figure supplement 2). The subembryonic and subcellular distributions of mRNAs for m^{6}A
466 methyltransferases and reading protein did not appear to be affected by ectopic expression of
467 MSL2 in aneuploid *Drosophila* embryos (Figure 1—figure supplement 2A-F; Figure 1—figure
468 supplement 2A'-F'). But the relative expression of m^{6}A components showed diverse dynamics,
469 among which the levels of the most important methyltransferase Ime4 are significantly

470 up-regulated in autosomal trisomy and sex chromosome trisomy with MSL2 overexpression
471 (Figure 7H; Figure 1—figure supplement 2A”-F”). Considering that unbalanced genomes can
472 affect the expression of MSL complex subunits, and the above results show that there is a close
473 relationship between MSL complex and m^6A modification, we speculate that unbalanced
474 genomes may influence the expression of m^6A regulators, possibly through the MSL complex.
475

476 **Relationship of H4K16Ac with m^6A modification**

477 As an important component of the MSL complex, MOF is a histone acetyltransferase that
478 specifically acetylates histone H4 at lysine 16 (H4K16Ac), thereby affecting chromatin structure
479 and functions, and activating transcription (Kind et al., 2008; Conrad et al., 2012). Previous
480 studies have elucidated the regulatory role of m^6A in histone modifications, and histone 3 lysine
481 36 trimethylation (H3K36me3) also plays a role in recruiting methyltransferase complexes to
482 deposit m^6A markers on RNA (Wang et al., 2018; Huang et al., 2019; Li et al., 2020). To investigate
483 the functions of MOF-mediated H4K16Ac on RNA m^6A modification, we analyzed RNA-seq data
484 from *Drosophila* strains overexpressing MOF (Figure 8A; Figure 7—figure supplement 1H-J). We
485 found obvious changes in the expression of m^6A regulators in strains overexpressing MOF, with
486 the levels of almost all m^6A regulators being elevated (Figure 8A). It was also observed that after
487 overexpression of MOF, the increasing trends of m^6A regulators in females and males were not
488 exactly the same, mostly showing more pronounced increases in females, except for Mettl3
489 (Ime4) and dMettl14. According to the results of RT-qPCR, the expression of Ythdc1 was
490 decreased in MOF knockdown strains and increased in MOF overexpression strains (Figure 8B;
491 Figure 7—figure supplement 1J); meanwhile, the expression levels of MOF were significantly
492 reduced in *Ythdc1* knockdown strains (Figure 8C). These results were further verified by polytene
493 chromosome immunofluorescence experiments (Figure 8D,E). In males, the expression level of
494 MOF was significantly decreased in *Ythdc1* knockdown *Drosophila*; while in *Ythdc1* knockdown
495 females, the expression level of MOF was not significantly changed compared with wildtype
496 females (Figure 8D,E). These results suggest that MOF-mediated acetylation modification can
497 have a certain effect on RNA m^6A methylation in a sexually dimorphic manner, which may be due
498 to the endogenous MSL complex and the imbalance of X chromosome dosage in males.

499 Next, we investigated whether the m^{6}A reader protein Ythdc1 would also have an effect on
500 the levels of H4K16Ac in *Drosophila*. Quantitative analysis of polytene chromosome
501 immunofluorescence results in *Ythdc1* knockdown *Drosophila* showed that the changes of
502 H4K16Ac levels also showed sexual dimorphism (Figure 8F,G). In males, knockdown of *Ythdc1* led
503 to a decrease in H4K16Ac level; whereas in females, knockdown of *Ythdc1* did not affect the level
504 of H4K16Ac (Figure 8F,G). These observed changes in H4K16Ac were consistent with the pattern
505 of changes in MOF protein in *Ythdc1* knockdown *Drosophila* strains, suggesting that m^{6}A
506 modification may affect H4K16Ac levels through the mediation of MOF. To further study whether
507 unbalanced genomes are involved in the interaction between m^{6}A and histone acetylation
508 modification, we also analyzed RNA sequencing data from trisomy 2L *Drosophila* strains
509 overexpressing MOF. The data showed that overexpression of MOF in trisomy 2L resulted in
510 significant changes in the expression of m^{6}A regulators, with a trend different from that observed
511 in diploids (Figure 8A). These results suggest that genomic imbalance might affect the interaction
512 between MOF and m^{6}A regulators to some extent, and the potential mechanisms require further
513 investigation.
514
515

516 ## Discussion

517 As an emerging epigenetic modification, RNA m^{6}A methylation has been found to be involved in
518 almost all aspects of RNA fate and metabolism (Gilbert et al., 2016; Yang et al., 2018). RNA m^{6}A
519 modification is also closely related to the development of organisms and a variety of human
520 diseases (Barbieri et al., 2017; Zhao et al., 2017; Pinello et al., 2018; Ma et al., 2019; Liu et al.,
521 2021; Shafik et al., 2021). However, the roles of m^{6}A methylation in development and gene
522 expression of aneuploidy have not been studied yet. Aneuploid variation is usually more
523 detrimental than changes of the entire chromosome set due to genomic imbalance (Birchler and
524 Veitia, 2007, 2012). The global changes of gene regulatory networks in unbalanced genomes
525 involves various epigenetic mechanisms, including histone modification, chromatin remodeling,
526 lncRNAs, microRNAs, etc. (Birchler, 2016; Zhang et al., 2021a, 2023; Shi et al., 2022). This study
527 demonstrated that the expression of m^{6}A components was altered under genomic imbalance,

528 leading to dynamic changes in the entire methylome. Potential intermediaries by which m^{6}A
529 modification could affect *trans* regulation and achieve dosage compensation in aneuploid
530 *Drosophila* were also investigated, such as dosage-sensitive modifiers, alternative splicing events,
531 and the MSL complex.

532 Our experiments show that the expression levels of most m^{6}A component genes are
533 significantly down-regulated in aneuploid *Drosophila* larvae (Figure 1A; Figure 1—figure
534 supplement 1C). Depletion of m^{6}A components interferes with the development of animals and
535 plants, especially leading to impaired self-renewal and differentiation of embryonic stem cells,
536 defects in embryonic development, and even early embryonic lethality (Granadino et al., 1990;
537 Horiuchi et al., 2006; Raffel et al., 2007; Luo et al., 2014; Wang Y et al., 2014; Geula et al., 2015).
538 We demonstrated by TSA-FISH that appropriate temporal and spatial specific distributions of the
539 transcripts for m^{6}A components are vital during *Drosophila* embryogenesis (Figure 1C-F; Figure
540 1—figure supplement 2). The abnormal expression of m^{6}A-related genes may affect the
541 development of aneuploid embryos.

542 In previous studies, the abundance of m^{6}A modification is usually positively correlated with
543 the number of m^{6}A peaks and m^{6}A-marked genes (Luo et al., 2014; Zhu et al., 2023). However,
544 our results obviously did not conform to this rule, with higher m^{6}A abundance and fewer
545 MeRIP-Seq peaks in aneuploids (Figure 2A-C). This reflects the complexity and heterogeneity of
546 m^{6}A modification. We suspect that in aneuploidy many RNAs may be lost that are methylated at
547 a low level in wildtype, and possess a higher proportion of highly methylated RNAs. Analysis of
548 the expression levels at each m^{6}A site confirmed our hypothesis (Figure 2D). Thus, this
549 phenomenon represents an imbalance in m^{6}A methylation caused by aneuploidy.

550 The distribution of m^{6}A sites on gene features, m^{6}A consensus motifs, biotypes of
551 m^{6}A-marked genes, enriched functions and pathways of methylated genes in aneuploidies are
552 similar to those in wildtype. We also found that genes highly methylated in all genotypes are
553 enriched for transcription factors (Figure 2I). It is consistent with previous studies suggesting that
554 transcription regulatory genes may be preferentially targeted by m^{6}A (Kan et al., 2017).

555 We also analyzed the characteristics of DMPs and DMP-associated genes in trisomies. By
556 observing the distributions of MeRIP-Seq reads around DMP sites, it can be found that the
557 densities of m^{6}A-marked reads on chromosome 2L are relatively higher in trisomy 2L females and

558 males (Figure 3F,G). Meanwhile, metafemales with triple X have a higher density of m^6A-marked
559 reads on chromosome X (Figure 3H). Previous studies have found that there is dosage
560 compensation for *cis*-genes in autosomal and sex chromosome aneuploid *Drosophila*, and the
561 expression of most genes on varied chromosomes approaches diploid levels (Sun et al., 2013b,c).
562 Therefore, the up-regulation of m^6A levels is not directly caused by the increased number of
563 chromosomes. A recent study found that the selective enrichment of m^6A methylation may play a
564 role as a transcript degradation signal in dosage compensation in mammals (Rücklé et al., 2023).
565 Therefore, we speculate that changes in m^6A levels in aneuploid *Drosophila* may affect its dosage
566 compensation and inverse dosage effect by regulating the stability of the transcripts. In addition,
567 more up-regulated DMPs are detected in trisomy 2L males and metafemales, while trisomy 2L
568 females have more down-regulated DMPs (Figure 3A-D). Combined with the fact that the survival
569 rate of trisomy 2L female larvae is relatively lower than that of the other two trisomies, it can be
570 speculated that the regulation of DMPs may affect the survival and development of aneuploid
571 *Drosophila*.

572 Gene expression in unbalanced genomes is extensively modulated (Sun et al., 2013b,c; Hou et
573 al., 2018; Raznahan et al., 2018; Shi et al., 2021; Yang et al., 2021; Zhang et al., 2021b; San Roman
574 et al., 2023). Previous studies have analyzed the transcriptome data of autosomal and sex
575 chromosome trisomic *Drosophila*, and found that most of the genes on the triple chromosomes
576 were compensated, and the ratios of their expression levels to wildtype were approximately 1;
577 meanwhile, the expression of genes on other chromosomes was close to two-thirds of that of the
578 wildtype, which was called an inverse dosage effect (Sun et al., 2013b,c; Zhang et al., 2021b). We
579 investigated the relationships between genes with different m^6A methylation status and genes
580 modulated by classical dosage-related effects (Figure 5F-H). The results showed that for
581 aneuploid females, genes methylated in both trisomy and control are significantly enriched in
582 dosage compensated *cis* genes and inverse dosage effect *trans* genes, and genes not methylated
583 at all are enriched in dosage effect genes. However, in aneuploid males, methylated genes are
584 associated with gene dosage effect (Figure 5F-H). We also found that the proportion of 5'UTR
585 m^6A peaks on dosage compensation and inverse dosage effect genes are increased in aneuploid
586 females (Figure 5I-K). These results provide evidence of sexual dimorphism in the relationships
587 between RNA m^6A modification and dosage-related effects. m^6A located in the 5'UTR generally

588 shows higher tissue specificity and richer dynamic changes, and may have unique regulatory
589 functions (Dominissini et al., 2012; Meyer and Jaffrey, 2014; Gilbert et al., 2016). The increased
590 proportion of m^6A in the 5'UTR of genes with classical dosage-related effects in aneuploidies
591 suggests that m^6A modification may be involved in the regulation of dosage-dependent genes.

592 Dosage-related effects of aneuploidy are thought to be caused by dosage-sensitive genes (Shi
593 et al., 2021; Yang et al., 2021). Some dosage-sensitive regulators have been identified in
594 *Drosophila*, and changes in the dosage of individual regulatory genes can mimic the effects of
595 aneuploidy in the whole genome (Birchler et al., 2001; Xie and Birchler, 2012; Zhang et al., 2021b).
596 Most dosage-sensitive regulators are transcription factors, signal transduction components, and
597 chromatin proteins, which have in common being members of macromolecular complexes or
598 having multicomponent interactions (Birchler et al., 2001; Birchler and Veitia, 2007). We studied
599 the m^6A modification of dosage-dependent genes and their protein-protein interaction networks
600 in aneuploid *Drosophila* (Figure 5—figure supplement 1). The results showed that there are
601 complex interactions between dosage-sensitive regulators and differentially expressed genes.
602 Among them, most of the DEGs located on the unvaried chromosomes are down-regulated,
603 indicating that the dosage-sensitive regulators mainly have negative effects on *trans* target genes.
604 There are more regulatory genes with up-regulated DMPs than down-regulated DMPs in all three
605 aneuploidies, and many of the regulators with up-regulated methylation are connected with
606 interactors that have down-regulated expression.

607 We comprehensively analyzed the relationships among RNA m^6A modification, gene
608 expression levels, and alternative splicing. The data showed that differential m^6A methylation
609 under genomic imbalance appeared to be more closely associated with differential alternative
610 splicing (Figure 5A-C; Figure 6A-C). This phenomenon is reasonable because the mutation or
611 knockout of *Ime4*, *dMettl14*, *fl(2)d*, and *Ythdc1* has been found to affect a large number of
612 alternative splicing events in *Drosophila*, and *fl(2)d* itself is thought to encode a splicing factor
613 (Penn et al., 2008; Haussmann et al., 2016; Lence et al., 2016). A small set of transcripts are
614 simultaneously differentially m^6A methylated, differentially expressed, and differentially
615 alternative spliced in aneuploidies, including the transcription factor *su(Hw)*, which may be a
616 dosage-sensitive regulator (Figure 6G-H). Besides, m^6A modification in the 5'UTR regions may
617 play a special role in some differential alternative splicing events (Figure 6—figure supplement

618 1F-I).

619 RNA m^6A modification in *Drosophila* has been shown to be involved in the alternative splicing
620 of *Sxl* (Lence et al., 2017). The deletion of some m^6A components in females will result in a
621 reduction of female-specific splicing of *Sxl* and an increase of the inclusion of the third exon,
622 along with phenotypic sexual transformation (Haussmann et al., 2016; Lence et al., 2016; Kan et
623 al., 2017). We found that *Sxl* transcripts of aneuploid *Drosophila* are both differentially m^6A
624 methylated and differentially spliced (Figure 7A-B). Among multiple alternative splicing events,
625 trisomy 2L females have a higher level of the third exon inclusion compared with wildtype
626 females (Figure 7B), which may be related to the differential methylation at 5'UTR of the *Sxl*
627 transcripts.

628 Some studies proposed that the deletion of RNA m^6A methyltransferase Ime4 harms the
629 survival of female *Drosophila* because of the insufficient inhibition of *msl-2* caused by decreased
630 *Sxl* levels, which in turn leads to up-regulation of X-linked genes (Haussmann et al., 2016).
631 However, other studies have found that the expression of genes on the X chromosome in females
632 with ectopic expression of MSL2 does not increase twofold, that is, the MSL complex does not
633 directly mediate dosage compensation, and the global inverse dosage effect caused by the
634 imbalance of sex chromosomes is the basis for dosage compensation (Birchler, 1981, 2016; Sun et
635 al., 2013a). Therefore, the lethality of the lack of m^6A in female *Drosophila* may not be directly
636 caused by up-regulation of X-linked genes through ectopic assembly of MSL complex, and the
637 specific reasons need to be further studied.

638 The functions of MSL complex in dynamic regulation of global gene expression in aneuploid
639 genomes has been described (Zhang et al., 2021a). Here, we found that MSL2, a structure
640 component of MSL complex, not only affects the expression of m^6A regulators, but also
641 influences the overall abundance of m^6A in *Drosophila* (Figure 7C-F), proving a close relationship
642 between the MSL complex and RNA m^6A modification. In addition, under the condition of
643 genomic imbalance, the relative expression of m^6A components was also changed in larvae and
644 embryos of MSL2-overexpressed trisomies (Figure 7G,H). Another component of the MSL
645 complex, MOF, which mediates histone acetylation and transcriptional activation (Kind et al.,
646 2008; Conrad et al., 2012), is also closely associated with the m^6A reader Ythdc1. Overexpression
647 of MOF increased the expression of Ythdc1 (Figure 8A,B), and in turn, knockdown of *Ythdc1*

648 reduced the expression of MOF and the level of H4K16Ac catalyzed by it (Figure 8C-G). These
649 results demonstrate complicated interactions between RNA m^6A methylation and the MSL
650 complex in unbalanced genomes, which may affect the gene expression, sexual dimorphism,
651 development and survival of aneuploid *Drosophila*.
652
653

654 Materials and methods

655 Key resources table

656 Softwares used in this study:

Resource	Designation	Source or reference
software, algorithm	R v4.2.2	http://www.R-project.org
software, algorithm	trim-galore v0.6.10	https://www.bioinformatics.babraham.ac.uk/projects/trim_galore/
software, algorithm	FastQC v0.12.1	https://www.bioinformatics.babraham.ac.uk/projects/fastqc/
software, algorithm	HISAT2 v2.2.1	Kim et al., 2019
software, algorithm	StringTie v2.1.5	Pertea et al., 2015
software, algorithm	exomePeak2 v1.10.0	Meng et al., 2013
software, algorithm	HOMER v4.11	Heinz et al., 2010
software, algorithm	DiffBind v3.8.4	Stark and Brown, 2013
software, algorithm	ChIPseeker v1.34.1	Yu et al., 2015
software, algorithm	deepTools v3.5.4	Ramírez et al., 2014
	rMATS v4.2.0	Shen et al., 2014
software, algorithm	ggplot2 v3.4.0	Villanueva and Chen, 2019
software, algorithm	clusterProfiler v4.6.0	Wu et al., 2021
software, algorithm	org.Dm.eg.db v3.16.0	https://www.bioconductor.org/
software, algorithm	DESeq2 v1.38.2	Love et al., 2014
software, algorithm	Integrative Genomics Viewer v2.12.0	Thorvaldsdóttir et al., 2013
software, algorithm	Fiji v1.53c	Schindelin et al., 2012
software, algorithm	AnimalTFDB	Hu et al., 2019

657

658 Antibodies used in this study:

Antibody	Manufacturer	Product #	RRID #
Mouse anti-SXL	Developmental Studies Hybridoma	M18-s	AB_528464

	Bank		
Goat anti-MSL2	Santa Cruz	sc-32459	AB_672213
Goat anti-MOF	Santa Cruz	sc-22351	AB_670132
Rabbit anti-H4K16Ac	EMD Millipore	07-329	AB_310525
Alexa Fluor 488/594	Jackson Immuno Research	N/A	N/A
Biotin-Conjugated Mouse Monoclonal Anti-Digoxigenin antibody	Jackson Immuno Research	200-062-156	AB_2339017
Streptavidin-HRP	Invitrogen	S991	N/A
Cyanine 3 Tyramide	Akoya Biosciences	FP1046	N/A

659

660 ## *Drosophila* stocks and genetic crosses

661 The *Drosophila* strains mentioned in this study were all maintained and crossed in our laboratory.
662 The crossing methods have been described previously (Zhang et al., 2021a). Trisomy
663 chromosome 2 left arm (2L) female and male third instar larvae were obtained from the cross of
664 *y; C(2L)dp; F(2R) bw* females and Canton S males. The metafemale larvae were obtained from the
665 cross of *C(1)DX, ywf/winscy* females and Canton S males. Aneuploidies overexpressing MSL2 were
666 generated from the crosses of *Drosophila* with compound chromosomes and MSL2 homozygotes.
667 The MSL2 transgene strain was constructed and validated in a previous study (Sun et al., 2013a).
668 All *Drosophila* strains were cultured on cornmeal dextrose medium at 25°C. Genes and
669 chromosomal balancers are described in Flybase (https://flybase.org/).

670

671 ## RNA m^6A methylation quantification

672 Total RNA was extracted from *Drosophila* larvae using TRIzol Reagent (Invitrogen) to detect the
673 abundance of m^6A. The relative quantification of m^6A methylation was performed using EpiQuik
674 m^6A RNA Methylation Quantification Kit (Colorimetric) (Epigentek, NY, USA, Cat # P-9005).
675 Specifically, 80 µl of Binding Solution was first added to each well of the plate, and 200 ng of RNA
676 samples, 2 µl of Negative Control, or 2 µl of diluted Positive Control were added to the designed
677 wells. Subsequently, the plate was incubated at 37°C for 90 min. After washing with Wash Buffer,
678 50 µl of Capture Antibody, 50 µl of Detection Antibody, and 50 µl of Enhancer Solution were
679 added to each well in order, and wells were emptied before adding a new solution each time.

680 Finally, 100 µl of Developer Solution and Stop Solution were added to each well away from light,
681 and the absorbance was read on a microplate reader at a wavelength of 450 nm.
682

683 **m^6A methylated RNA immunoprecipitation sequencing (MeRIP-Seq)**

684 The MeRIP-Seq service was provided by Cloudseq Biotech Inc. (Shanghai, China), and this
685 technology was developed on the basis of published experimental methods (Meyer et al., 2012).
686 In brief, *Drosophila* larvae of five genotypes, each with two biological replicates, were collected
687 for sequencing. Ribosomal RNAs were removed from total RNA using Ribo-Zero rRNA Removal
688 Kits (Illumina, USA). Immunoprecipitation of m^6A RNA was performed using GenSeq® m^6A RNA IP
689 kit (GenSeq, Shanghai, China). The NEBNext® Ultra II Directional RNA Library Prep kit (New
690 England Biolabs, USA) was used for RNA sequencing library construction. High-throughput
691 sequencing was performed using Illumina NovaSeq 6000 sequencers with the paired-end 150 bp
692 protocol.
693

694 **Analysis of MeRIP-Seq data**

695 The raw sequencing data was first filtered by Trim Galore (version 0.6.10)
696 (https://www.bioinformatics.babraham.ac.uk/projects/trim_galore/) to remove adapters and
697 low-quality reads. The quality of the data was then assessed by FastQC (version 0.12.1)
698 (https://www.bioinformatics.babraham.ac.uk/projects/fastqc/). Subsequently, clean reads were
699 aligned to the *Drosophila* reference genome (Drosophila_melanogaster.BDGP6.32.dna.toplevel.fa,
700 downloaded from the Ensembl database) using HISAT2 (version 2.2.1) (Kim et al., 2019). Next,
701 The R package exomePeak2 (version 1.10.0) (Meng et al., 2013) was used for m^6A peak calling
702 (the screening criteria were log2FC ≥ 1, RPM.IP ≥ 0.5, and score ≥ 5). Motif analysis was
703 performed using HOMER (version 4.11) (Heinz et al., 2010). Differentially methylated peaks were
704 analyzed by the R package DiffBind (version 3.8.4) (Stark and Brown, 2013), which employs the
705 DESeq2 (Love et al., 2014) method. m^6A peaks with a p-value of 0.1 or less were considered as
706 differentially methylated peaks (DMPs). ChIPseeker (version 1.34.1) (Yu et al., 2015) was used to
707 annotate the peaks, and plotted some of the figures. The profiles and heatmaps of MeRIP-Seq
708 reads around DMPs were generated by deepTools (version 3.5.4) (Ramírez et al., 2014). The signal

709 distribution on the genome was visualized using the Integrative Genomics Viewer (IGV) software
710 (version 2.12.0) (Thorvaldsdóttir et al., 2013).
711

712 **RNA sequencing data and analysis**

713 The RNA-seq data of aneuploid *Drosophila* used in this article were generated in a previous study
714 (Zhang et al., 2023) and can be downloaded from the Gene Expression Omnibus (GEO) database
715 (GSE233534). Genome mapping of sequencing data and gene expression quantification were
716 carried out through HISAT2-StringTie pipeline (Pertea et al., 2015; Kim et al., 2019). Differential
717 alternative splicing events were identified by rMATS (version 4.2.0) program (Shen et al., 2014)
718 (with the parameters of -t paired --readLength 150 --cstat 0.0001 --libType fr-firststrand). The
719 method of generating the ratio distributions of gene expression changes was as described
720 previously (Zhang et al., 2022). The plots were generated using ggplot2 (version 3.4.0) (Villanueva
721 and Chen, 2019) in the R program (version 4.2.2). Differential expression analysis was performed
722 by DESeq2 (version 1.38.2) (Love et al., 2014), and the threshold was set to adjusted p-value ≤
723 0.05. The functional enrichment analysis was performed by ClusterProfiler (version 4.6.0) (Wu et
724 al., 2021) based on org.Dm.eg.db (version 3.16.0) from Bioconductor
725 (https://www.bioconductor.org/). The Kyoto Encyclopedia of Genes and Genomes (KEGG)
726 pathway data was obtained from the network (https://www.kegg.jp/). The list of transcription
727 factors of *Drosophila* was downloaded from AnimalTFDB (Hu et al., 2019). Protein-protein
728 interaction (PPI) relationships were obtained from the STRING database (Szklarczyk et al., 2019).
729

730 **Real-time quantitative PCR**

731 Total RNA of *Drosophila* whole larvae, larval brains, or adult heads was extracted using TRIzol
732 Reagent (Invitrogen), and reverse transcription was done with *TransScript* one-step gDNA
733 Removal and cDNA Synthesis SuperMix (TransGen Biotech). The sequences of primers designed
734 for RT-qPCR were listed in Figure 1—figure supplement 1A. The usability of these primers was
735 verified by agarose gel electrophoresis (Figure 1—figure supplement 1B). The real-time PCR was
736 performed with *TransStart* Tip Green qPCR SuperMix (+ Dye II) (TransGen Biotech) using ABI
737 QuantStudio 6 Flex Real-Time PCR System. Relative quantification of gene expression was

738 determined using the $2^{-\Delta\Delta Ct}$ method.

739

740 **Fluorescence *in situ* hybridization (FISH) of *Drosophila* embryos**

741 Collection of *Drosophila* embryos and fluorescence *in situ* hybridization were performed as
742 previously described (Jandura et al., 2017; Zhang et al., 2021a). The probe primers containing
743 flanking T7 promoter elements were listed in Figure 1—figure supplement 1D. After PCR
744 amplification and *in vitro* transcription, their products were examined by agarose gel
745 electrophoresis (Figure 1—figure supplement 1E). Digoxygenin (DIG)-labelled antisense RNA
746 probes were hybridized to transcripts of interest, and then detected using a succession of
747 anti-DIG antibody conjugated to biotin, streptavidin conjugated to horseradish peroxidase (HRP)
748 and fluorescently conjugated tyramide. This hierarchical process can greatly enhance the probe
749 signals and is referred to as a tyramide signal amplification (TSA) system. All images were
750 acquired with a Zeiss LSM880 laser confocal fluorescence microscope using ZEN software. The
751 same probes for relative fluorescence intensity analysis were photographed using the same
752 parameters. Fluorescence images were processed and analyzed using Fiji (version 1.53c)
753 (Schindelin et al., 2012).

754

755 **Polytene chromosomes immunostaining**

756 Salivary gland chromosomes immunostaining was performed as previously described (Zhang et
757 al., 2021a). Briefly speaking, the salivary glands from third-instar larvae were first fixed in 3.7%
758 formaldehyde for 1 min, and then dissociated with 50% acetic acid for 5 min. Polytene
759 chromosomes were treated with the following primary antibodies at a dilution of 1:100: anti-SXL
760 (Developmental Studies Hybridoma Bank, M18-s), anti-MSL2 (Santa Cruz, sc-32459), anti-MOF
761 (Santa Cruz, sc-22351), and anti-H4K16Ac (EMD Millipore, 07-329). Finally,
762 fluorescence-conjugated secondary antibodies (Alexa Fluor 488 and Alexa Fluor 594, Jackson
763 Immuno Research) were used for detection.

764

765

Acknowledgements

This work was supported by National Natural Science Foundation of China (Grant No. 31871243 and No. 32070566) to L.S. We thank James A.Birchler for revising the manuscript.

Additional information

Funding

Funder	Grant reference number	Author
National Natural Science Foundation of China	No. 31871243	Lin Sun
National Natural Science Foundation of China	No. 32070566	Lin Sun

Author contributions

Shuai Zhang: Methodology, Investigation, Data Curation, Formal analysis, Writing - Original Draft, Writing - Review & Editing, Visualization. Xinyu Liu, Methodology, Investigation, Validation, Writing - Original Draft, Writing - Review & Editing, Visualization. Ruixue Wang, Methodology, Investigation, Validation, Writing - Original Draft, Writing - Review & Editing, Visualization. Junhan Wang: Methodology, Investigation, Formal analysis. Ludan Zhang: Methodology, Investigation, Validation. Lin Sun: Conceptualization, Writing - Original Draft, Writing - Review & Editing, Supervision, Project administration, Funding acquisition. All authors have read and approved the final manuscript.

Additional files

Supplementary files

Supplementary File 1

Data availability

All raw and processed sequencing data generated in this study have been submitted to the NCBI Gene Expression Omnibus (GEO; https://www.ncbi.nlm.nih.gov/geo/) under accession number GSE253401. The previously published RNA-seq data used in this study are available at the GEO repository under the accession number GSE233534.

The following datasets were generated:

Author(s)	Year	Dataset title	Dataset URL	Database and Identifier
Zhang S, Liu X, Wang R, Wang J, Zhang L, Sun L	2024	Dynamics and regulatory roles of RNA m^6A methylation in unbalanced genomes	https://www.ncbi.nlm.nih.gov/geo/query/acc.cgi?acc=GSE253401	NCBI Gene Expression Omnibus, GSE253401

The following previously published datasets were used:

Author(s)	Year	Dataset title	Dataset URL	Database and Identifier
Zhang S, Wang R, Zhu X, Zhang L, Liu X, Sun L	2024	Characteristics and expression of lncRNA in *Drosophila* aneuploidy	https://www.ncbi.nlm.nih.gov/geo/query/acc.cgi?acc=GSE233534	NCBI Gene Expression Omnibus, GSE233534

References

Barbieri, I., Tzelepis, K., Pandolfini, L., Shi, J., Millan-Zambrano, G., Robson, S. C., Aspris, D., Migliori, V., Bannister, A. J., Han, N., De Braekeleer, E., Ponstingl, H., Hendrick, A., Vakoc, C. R., Vassiliou, G. S., & Kouzarides, T. (2017). Promoter-bound METTL3 maintains myeloid leukaemia by m(6)A-dependent translation control. *Nature*, *552*(7683), 126-131. https://doi.org/10.1038/nature24678

Ben-David, U., & Amon, A. (2020). Context is everything: aneuploidy in cancer. *Nature Reviews Genetics*, *21*(1), 44-62. https://doi.org/10.1038/s41576-019-0171-x

Birchler, J. A. (1981). The genetic basis of dosage compensation of alcohol dehydrogenase-1 in maize. *Genetics*, *97*(3-4), 625-637. https://www.ncbi.nlm.nih.gov/pubmed/17249082

Birchler, J. A. (2016). Parallel Universes for Models of X Chromosome Dosage Compensation in *Drosophila*: A Review. *Cytogenetic and Genome Research*, *148*(1), 52-67. https://doi.org/10.1159/000445924

Birchler, J. A., Bhadra, U., Bhadra, M. P., & Auger, D. L. (2001). Dosage-dependent gene regulation in multicellular eukaryotes: implications for dosage compensation, aneuploid syndromes, and quantitative traits. *Developmental Biology*, *234*(2), 275-288. https://doi.org/10.1006/dbio.2001.0262

Birchler, J. A., & Veitia, R. A. (2007). The gene balance hypothesis: from classical genetics to modern genomics. *Plant Cell*, *19*(2), 395-402. https://doi.org/10.1105/tpc.106.049338

Birchler, J. A., & Veitia, R. A. (2012). Gene balance hypothesis: connecting issues of dosage sensitivity across biological disciplines. *Proceedings of the National Academy of Sciences of the United States of America*, *109*(37), 14746-14753. https://doi.org/10.1073/pnas.1207726109

Birchler, J. A., & Veitia, R. A. (2021). One Hundred Years of Gene Balance: How Stoichiometric Issues Affect Gene Expression, Genome Evolution, and Quantitative Traits. *Cytogenetic and Genome Research*, *161*(10-11), 529-550. https://doi.org/10.1159/000519592

Chiarle, R. (2021). Solving the chromosome puzzle of aneuploidy in cancer. *Genes Dev*, *35*(15-16), 1073-1075. https://doi.org/10.1101/gad.348773.121

Conrad, T., Cavalli, F. M. G., Holz, H., Hallacli, E., Kind, J., Ilik, I., Vaquerizas, J. M., Luscombe, N. M., & Akhtar, A. (2012). The MOF Chromobarrel Domain Controls Genome-wide H4K16 Acetylation and Spreading of the MSL Complex. *Developmental Cell*, *22*(3), 610-624. https://doi.org/10.1016/j.devcel.2011.12.016

Disteche, C. M. (2016). Dosage compensation of the sex chromosomes and autosomes. *Semin Cell Dev Biol*, *56*, 9-18. https://doi.org/10.1016/j.semcdb.2016.04.013

Dominissini, D., Moshitch-Moshkovitz, S., Schwartz, S., Salmon-Divon, M., Ungar, L., Osenberg, S., Cesarkas, K., Jacob-Hirsch, J., Amariglio, N., Kupiec, M., Sorek, R., & Rechavi, G. (2012). Topology of the human and mouse m6A RNA methylomes revealed by m6A-seq. *Nature*, *485*(7397), 201-206. https://doi.org/10.1038/nature11112

Geula, S., Moshitch-Moshkovitz, S., Dominissini, D., Mansour, A. A., Kol, N., Salmon-Divon, M., Hershkovitz, V., Peer, E., Mor, N., Manor, Y. S., Ben-Haim, M. S., Eyal, E., Yunger, S., Pinto, Y.,

Jaitin, D. A., Viukov, S., Rais, Y., Krupalnik, V., Chomsky, E., . . . Hanna, J. H. (2015). Stem cells. m6A mRNA methylation facilitates resolution of naive pluripotency toward differentiation. *Science*, *347*(6225), 1002-1006. https://doi.org/10.1126/science.1261417

Gilbert, W. V., Bell, T. A., & Schaening, C. (2016). Messenger RNA modifications: Form, distribution, and function. *Science*, *352*(6292), 1408-1412. https://doi.org/10.1126/science.aad8711

Granadino, B., Campuzano, S., & Sanchez, L. (1990). The *Drosophila melanogaster fl(2)d* gene is needed for the female-specific splicing of *Sex-lethal* RNA. *EMBO Journal*, *9*(8), 2597-2602. https://doi.org/DOI 10.1002/j.1460-2075.1990.tb07441.x

Gurudatta, B. V., Ramos, E., & Corces, V. G. (2012). The BEAF insulator regulates genes involved in cell polarity and neoplastic growth. *Developmental Biology*, *369*(1), 124-132. https://doi.org/10.1016/j.ydbio.2012.06.013

Haussmann, I. U., Bodi, Z., Sanchez-Moran, E., Mongan, N. P., Archer, N., Fray, R. G., & Soller, M. (2016). m(6)A potentiates *Sxl* alternative pre-mRNA splicing for robust *Drosophila* sex determination. *Nature*, *540*(7632), 301-304. https://doi.org/10.1038/nature20577

Heinz, S., Benner, C., Spann, N., Bertolino, E., Lin, Y. C., Laslo, P., Cheng, J. X., Murre, C., Singh, H., & Glass, C. K. (2010). Simple Combinations of Lineage-Determining Transcription Factors Prime *cis*-Regulatory Elements Required for Macrophage and B Cell Identities. *Molecular Cell*, *38*(4), 576-589. https://doi.org/10.1016/j.molcel.2010.05.004

Hongay, C. F., & Orr-Weaver, T. L. (2011). *Drosophila* Inducer of MEiosis 4 (*IME4*) is required for Notch signaling during oogenesis. *Proceedings of the National Academy of Sciences of the United States of America*, *108*(36), 14855-14860. https://doi.org/10.1073/pnas.1111577108

Horiuchi, K., Umetani, M., Minami, T., Okayama, H., Takada, S., Yamamoto, M., Aburatani, H., Reid, P. C., Housman, D. E., Hamakubo, T., & Kodama, T. (2006). Wilms' tumor 1-associating protein regulates G2/M transition through stabilization of cyclin A2 mRNA. *Proceedings of the National Academy of Sciences of the United States of America*, *103*(46), 17278-17283. https://doi.org/10.1073/pnas.0608357103

Hou, J., Shi, X., Chen, C., Islam, M. S., Johnson, A. F., Kanno, T., Huettel, B., Yen, M. R., Hsu, F. M., Ji, T., Chen, P. Y., Matzke, M., Matzke, A. J. M., Cheng, J., & Birchler, J. A. (2018). Global impacts of chromosomal imbalance on gene expression in *Arabidopsis* and other taxa. *Proceedings of the National Academy of Sciences of the United States of America*, *115*(48), E11321-E11330.

870 https://doi.org/10.1073/pnas.1807796115

871 Hu, H., Miao, Y. R., Jia, L. H., Yu, Q. Y., Zhang, Q., & Guo, A. Y. (2019). AnimalTFDB 3.0: a
872 comprehensive resource for annotation and prediction of animal transcription factors. *Nucleic*
873 *Acids Research*, *47*(D1), D33-D38. https://doi.org/10.1093/nar/gky822

874 Huang, A. C., Olson, S. B., & Maslen, C. L. (2021). A Review of Recent Developments in Turner
875 Syndrome Research. *J Cardiovasc Dev Dis*, *8*(11), 475-491.
876 https://doi.org/10.3390/jcdd8110138

877 Huang, H., Weng, H., Zhou, K., Wu, T., Zhao, B. S., Sun, M., Chen, Z., Deng, X., Xiao, G., Auer, F.,
878 Klemm, L., Wu, H., Zuo, Z., Qin, X., Dong, Y., Zhou, Y., Qin, H., Tao, S., Du, J., . . . Chen, J. (2019).
879 Histone H3 trimethylation at lysine 36 guides m(6)A RNA modification co-transcriptionally.
880 *Nature*, *567*(7748), 414-419. https://doi.org/10.1038/s41586-019-1016-7

881 Jaenisch, R., & Bird, A. (2003). Epigenetic regulation of gene expression: how the genome
882 integrates intrinsic and environmental signals. *Nature Genetics*, *33 Suppl*, 245-254.
883 https://doi.org/10.1038/ng1089

884 Jandura, A., Hu, J., Wilk, R., & Krause, H. M. (2017). High Resolution Fluorescent *In Situ*
885 Hybridization in Drosophila Embryos and Tissues Using Tyramide Signal Amplification. *J Vis*
886 *Exp*, *128*(128), 56281. https://doi.org/10.3791/56281

887 Jordan, W., Rieder, L. E., & Larschan, E. (2019). Diverse Genome Topologies Characterize Dosage
888 Compensation across Species. *Trends in Genetics*, *35*(4), 308-315.
889 https://doi.org/10.1016/j.tig.2019.02.001

890 Kan, L., Grozhik, A. V., Vedanayagam, J., Patil, D. P., Pang, N., Lim, K. S., Huang, Y. C., Joseph, B., Lin,
891 C. J., Despic, V., Guo, J., Yan, D., Kondo, S., Deng, W. M., Dedon, P. C., Jaffrey, S. R., & Lai, E. C.
892 (2017). The m(6)A pathway facilitates sex determination in *Drosophila*. *Nat Commun*, *8*,
893 15737. https://doi.org/10.1038/ncomms15737

894 Kim, D., Paggi, J. M., Park, C., Bennett, C., & Salzberg, S. L. (2019). Graph-based genome
895 alignment and genotyping with HISAT2 and HISAT-genotype. *Nature Biotechnology*, *37*(8),
896 907-915. https://doi.org/10.1038/s41587-019-0201-4

897 Kind, J., Vaquerizas, J. M., Gebhardt, P., Gentzel, M., Luscombe, N. M., Bertone, P., & Akhtar, A.
898 (2008). Genome-wide analysis reveals MOF as a key regulator of dosage compensation and
899 gene expression in *Drosophila*. *Cell*, *133*(5), 813-828.

900 https://doi.org/10.1016/j.cell.2008.04.036

901 Lecuyer, E., Yoshida, H., Parthasarathy, N., Alm, C., Babak, T., Cerovina, T., Hughes, T. R., Tomancak,
902 P., & Krause, H. M. (2007). Global analysis of mRNA localization reveals a prominent role in
903 organizing cellular architecture and function. *Cell*, *131*(1), 174-187.
904 https://doi.org/10.1016/j.cell.2007.08.003

905 Lee, M., Kim, B., & Kim, V. N. (2014). Emerging roles of RNA modification: m(6)A and U-tail. *Cell*,
906 *158*(5), 980-987. https://doi.org/10.1016/j.cell.2014.08.005

907 Lence, T., Akhtar, J., Bayer, M., Schmid, K., Spindler, L., Ho, C. H., Kreim, N., Andrade-Navarro, M.
908 A., Poeck, B., Helm, M., & Roignant, J. Y. (2016). m(6)A modulates neuronal functions and sex
909 determination in *Drosophila*. *Nature*, *540*(7632), 242-247.
910 https://doi.org/10.1038/nature20568

911 Lence, T., Soller, M., & Roignant, J. Y. (2017). A fly view on the roles and mechanisms of the m(6)A
912 mRNA modification and its players. *RNA Biology*, *14*(9), 1232-1240.
913 https://doi.org/10.1080/15476286.2017.1307484

914 Letourneau, A., Santoni, F. A., Bonilla, X., Sailani, M. R., Gonzalez, D., Kind, J., Chevalier, C.,
915 Thurman, R., Sandstrom, R. S., Hibaoui, Y., Garieri, M., Popadin, K., Falconnet, E., Gagnebin,
916 M., Gehrig, C., Vannier, A., Guipponi, M., Farinelli, L., Robyr, D., . . . Antonarakis, S. E. (2014).
917 Domains of genome-wide gene expression dysregulation in Down's syndrome. *Nature*,
918 *508*(7496), 345-350. https://doi.org/10.1038/nature13200

919 Li, Y., Xia, L., Tan, K., Ye, X., Zuo, Z., Li, M., Xiao, R., Wang, Z., Liu, X., Deng, M., Cui, J., Yang, M., Luo,
920 Q., Liu, S., Cao, X., Zhu, H., Liu, T., Hu, J., Shi, J., . . . Xia, L. (2020). *N*6-Methyladenosine
921 co-transcriptionally directs the demethylation of histone H3K9me2. *Nature Genetics*.
922 https://doi.org/10.1038/s41588-020-0677-3

923 Liu, J., Gao, M., He, J., Wu, K., Lin, S., Jin, L., Chen, Y., Liu, H., Shi, J., Wang, X., Chang, L., Lin, Y.,
924 Zhao, Y. L., Zhang, X., Zhang, M., Luo, G. Z., Wu, G., Pei, D., Wang, J., . . . Chen, J. (2021). The
925 RNA m(6)A reader YTHDC1 silences retrotransposons and guards ES cell identity. *Nature*,
926 *591*(7849), 322-326. https://doi.org/10.1038/s41586-021-03313-9

927 Love, M. I., Huber, W., & Anders, S. (2014). Moderated estimation of fold change and dispersion
928 for RNA-seq data with DESeq2. *Genome Biology*, *15*(12), 550.
929 https://doi.org/10.1186/s13059-014-0550-8

930 Lucchesi, J. C. (2018). Transcriptional modulation of entire chromosomes: dosage compensation.
931 *Journal of Genetics*, *97*(2), 357-364. https://doi.org/10.1007/s12041-018-0919-7
932 Luo, G. Z., MacQueen, A., Zheng, G., Duan, H., Dore, L. C., Lu, Z., Liu, J., Chen, K., Jia, G., Bergelson,
933 J., & He, C. (2014). Unique features of the m6A methylome in *Arabidopsis thaliana*. *Nat*
934 *Commun*, *5*, 5630. https://doi.org/10.1038/ncomms6630
935 Ma, S., Chen, C., Ji, X., Liu, J., Zhou, Q., Wang, G., Yuan, W., Kan, Q., & Sun, Z. (2019). The interplay
936 between m6A RNA methylation and noncoding RNA in cancer. *Journal of Hematology &*
937 *Oncology*, *12*(1), 121. https://doi.org/10.1186/s13045-019-0805-7
938 Meng, J., Cui, X. D., Rao, M. K., Chen, Y. D., & Huang, Y. F. (2013). Exome-based analysis for RNA
939 epigenome sequencing data. *Bioinformatics*, *29*(12), 1565-1567.
940 https://doi.org/10.1093/bioinformatics/btt171
941 Meyer, K. D., & Jaffrey, S. R. (2014). The dynamic epitranscriptome: *N*6-methyladenosine and
942 gene expression control. *Nature Reviews: Molecular Cell Biology*, *15*(5), 313-326.
943 https://doi.org/10.1038/nrm3785
944 Meyer, K. D., Patil, D. P., Zhou, J., Zinoviev, A., Skabkin, M. A., Elemento, O., Pestova, T. V., Qian, S.
945 B., & Jaffrey, S. R. (2015). 5′ UTR m6A Promotes Cap-Independent Translation. *Cell*, *163*(4),
946 999-1010. https://doi.org/10.1016/j.cell.2015.10.012
947 Meyer, K. D., Saletore, Y., Zumbo, P., Elemento, O., Mason, C. E., & Jaffrey, S. R. (2012).
948 Comprehensive analysis of mRNA methylation reveals enrichment in 3' UTRs and near stop
949 codons. *Cell*, *149*(7), 1635-1646. https://doi.org/10.1016/j.cell.2012.05.003
950 Orr, B., Godek, K. M., & Compton, D. (2015). Aneuploidy. *Current Biology*, *25*(13), R538-R542.
951 https://doi.org/10.1016/j.cub.2015.05.010
952 Park, S. W., Oh, H., Lin, Y. R., & Park, Y. (2010). MSL *cis*-spreading from *roX* gene up-regulates the
953 neighboring genes. *Biochem Biophys Res Commun*, *399*(2), 227-231.
954 https://doi.org/10.1016/j.bbrc.2010.07.059
955 Patil, D. P., Chen, C. K., Pickering, B. F., Chow, A., Jackson, C., Guttman, M., & Jaffrey, S. R. (2016).
956 m(6)A RNA methylation promotes *XIST*-mediated transcriptional repression. *Nature*,
957 *537*(7620), 369-373. https://doi.org/10.1038/nature19342
958 Penn, J. K., Graham, P., Deshpande, G., Calhoun, G., Chaouki, A. S., Salz, H. K., & Schedl, P. (2008).
959 Functioning of the *Drosophila* Wilms'-tumor-1-associated protein homolog, *Fl(2)d*, in

Sex-lethal-dependent alternative splicing. *Genetics*, *178*(2), 737-748. https://doi.org/10.1534/genetics.107.081679

Pertea, M., Pertea, G. M., Antonescu, C. M., Chang, T. C., Mendell, J. T., & Salzberg, S. L. (2015). StringTie enables improved reconstruction of a transcriptome from RNA-seq reads. *Nature Biotechnology*, *33*(3), 290-295. https://doi.org/10.1038/nbt.3122

Pinello, N., Sun, S., & Wong, J. J. (2018). Aberrant expression of enzymes regulating m(6)A mRNA methylation: implication in cancer. *Cancer Biol Med*, *15*(4), 323-334. https://doi.org/10.20892/j.issn.2095-3941.2018.0365

Prestel, M., Feller, C., & Becker, P. B. (2010). Dosage compensation and the global re-balancing of aneuploid genomes. *Genome Biology*, *11*(8), 216. https://doi.org/10.1186/gb-2010-11-8-216

Rabinow, L., & Birchler, J. A. (1989). A dosage-sensitive modifier of retrotransposon-induced alleles of the *Drosophila white* locus. *EMBO Journal*, *8*(3), 879-889. https://www.ncbi.nlm.nih.gov/pubmed/2542025

Raffel, G. D., Mercher, T., Shigematsu, H., Williams, I. R., Cullen, D. E., Akashi, K., Bernard, O. A., & Gilliland, D. G. (2007). *Ott1*(*Rbm15*) has pleiotropic roles in hematopoietic development. *Proceedings of the National Academy of Sciences of the United States of America*, *104*(14), 6001-6006. https://doi.org/10.1073/pnas.0609041104

Ramírez, F., Dündar, F., Diehl, S., Grüning, B. A., & Manke, T. (2014). deepTools: a flexible platform for exploring deep-sequencing data. *Nucleic Acids Research*, *42*(W1), W187-W191. https://doi.org/10.1093/nar/gku365

Raznahan, A., Parikshak, N. N., Chandran, V., Blumenthal, J. D., Clasen, L. S., Alexander-Bloch, A. F., Zinn, A. R., Wangsa, D., Wise, J., Murphy, D. G. M., Bolton, P. F., Ried, T., Ross, J., Giedd, J. N., & Geschwind, D. H. (2018). Sex-chromosome dosage effects on gene expression in humans. *Proceedings of the National Academy of Sciences of the United States of America*, *115*(28), 7398-7403. https://doi.org/10.1073/pnas.1802889115

Roseman, R. R., Pirrotta, V., & Geyer, P. K. (1993). The *su(Hw)* protein insulates expression of the *Drosophila melanogaster white* gene from chromosomal position-effects. *EMBO Journal*, *12*(2), 435-442. https://doi.org/DOI 10.1002/j.1460-2075.1993.tb05675.x

Roundtree, I. A., Evans, M. E., Pan, T., & He, C. (2017a). Dynamic RNA Modifications in Gene Expression Regulation. *Cell*, *169*(7), 1187-1200. https://doi.org/10.1016/j.cell.2017.05.045

990 Roundtree, I. A., Luo, G. Z., Zhang, Z. J., Wang, X., Zhou, T., Cui, Y. Q., Sha, J. H., Huang, X. X.,
991 Guerrero, L., Xie, P., He, E., Shen, B., & He, C. (2017b). YTHDC1 mediates nuclear export of
992 *N*6-methyladenosine methylated mRNAs. *Elife*, *6*, e31311. https://doi.org/ARTN e31311
993 Rücklé, C., Körtel, N., Basilicata, M. F., Busch, A., Zhou, Y., Hoch-Kraft, P., Tretow, K., Kielisch, F.,
994 Bertin, M., Pradhan, M., Musheev, M., Schweiger, S., Niehrs, C., Rausch, O., Zarnack, K.,
995 Valsecchi, C. I. K., & König, J. (2023). RNA stability controlled by m(6)A methylation
996 contributes to X-to-autosome dosage compensation in mammals. *Nature Structural &*
997 *Molecular Biology*, *30*(8). https://doi.org/10.1038/s41594-023-00997-7
998 San Roman, A. K., Godfrey, A. K., Skaletsky, H., Bellott, D. W., Groff, A. F., Harris, H. L., Blanton, L.
999 V., Hughes, J. F., Brown, L., Phou, S., Buscetta, A., Kruszka, P., Banks, N., Dutra, A., Pak, E.,
1000 Lasutschinkow, P. C., Keen, C., Davis, S. M., Tartaglia, N. R., . . . Page, D. C. (2023). The human
1001 inactive X chromosome modulates expression of the active X chromosome. *Cell Genom*, *3*(2),
1002 100259. https://doi.org/10.1016/j.xgen.2023.100259
1003 Sanchez-Pavon, E., Mendoza, H., & Garcia-Ferreyra, J. (2021). Trisomy 21 and Assisted
1004 Reproductive Technologies: A review. *JBRA Assist Reprod*, *26*(1), 129-141.
1005 https://doi.org/10.5935/1518-0557.20210047
1006 Schindelin, J., Arganda-Carreras, I., Frise, E., Kaynig, V., Longair, M., Pietzsch, T., Preibisch, S.,
1007 Rueden, C., Saalfeld, S., Schmid, B., Tinevez, J. Y., White, D. J., Hartenstein, V., Eliceiri, K.,
1008 Tomancak, P., & Cardona, A. (2012). Fiji: an open-source platform for biological-image analysis.
1009 *Nature Methods*, *9*(7), 676-682. https://doi.org/10.1038/Nmeth.2019
1010 Shafik, A. M., Zhang, F., Guo, Z., Dai, Q., Pajdzik, K., Li, Y., Kang, Y., Yao, B., Wu, H., He, C., Allen, E.
1011 G., Duan, R., & Jin, P. (2021). *N*6-methyladenosine dynamics in neurodevelopment and aging,
1012 and its potential role in Alzheimer's disease. *Genome Biology*, *22*(1), 17.
1013 https://doi.org/10.1186/s13059-020-02249-z
1014 Shen, S. H., Park, J. W., Lu, Z. X., Lin, L., Henry, M. D., Wu, Y. N., Zhou, Q., & Xing, Y. (2014). rMATS:
1015 Robust and flexible detection of differential alternative splicing from replicate RNA-Seq data.
1016 *Proceedings of the National Academy of Sciences of the United States of America*, *111*(51),
1017 E5593-E5601. https://doi.org/10.1073/pnas.1419161111
1018 Shi, X., Yang, H., Chen, C., Hou, J., Hanson, K. M., Albert, P. S., Ji, T., Cheng, J., & Birchler, J. A.
1019 (2021). Genomic imbalance determines positive and negative modulation of gene expression

in diploid maize. *Plant Cell*, *33*(4), 917-939. https://doi.org/10.1093/plcell/koab030

Shi, X., Yang, H., Chen, C., Hou, J., Ji, T., Cheng, J., & Birchler, J. A. (2022). Dosage-sensitive miRNAs trigger modulation of gene expression during genomic imbalance in maize. *Nat Commun*, *13*(1), 3014. https://doi.org/10.1038/s41467-022-30704-x

Stark, R., Brown, G. (2013). DiffBind: differential binding analysis of ChIP-seq peak data. *Bioconductor package*. http://www.bioconductor.org. DOI: 10.18129/B9.bioc.DiffBind.

Sun, L., Fernandez, H. R., Donohue, R. C., Li, J., Cheng, J., & Birchler, J. A. (2013a). Male-specific lethal complex in *Drosophila* counteracts histone acetylation and does not mediate dosage compensation. *Proceedings of the National Academy of Sciences of the United States of America*, *110*(9), E808-E817. https://doi.org/10.1073/pnas.1222542110

Sun, L., Johnson, A. F., Donohue, R. C., Li, J., Cheng, J., & Birchler, J. A. (2013b). Dosage compensation and inverse effects in triple X metafemales of *Drosophila*. *Proceedings of the National Academy of Sciences of the United States of America*, *110*(18), 7383-7388. https://doi.org/10.1073/pnas.1305638110

Sun, L., Johnson, A. F., Li, J., Lambdin, A. S., Cheng, J., & Birchler, J. A. (2013c). Differential effect of aneuploidy on the X chromosome and genes with sex-biased expression in *Drosophila*. *Proceedings of the National Academy of Sciences of the United States of America*, *110*(41), 16514-16519. https://doi.org/10.1073/pnas.1316041110

Szklarczyk, D., Gable, A. L., Lyon, D., Junge, A., Wyder, S., Huerta-Cepas, J., Simonovic, M., Doncheva, N. T., Morris, J. H., Bork, P., Jensen, L. J., & Mering, C. (2019). STRING v11: protein-protein association networks with increased coverage, supporting functional discovery in genome-wide experimental datasets. *Nucleic Acids Research*, *47*(D1), D607-D613. https://doi.org/10.1093/nar/gky1131

Thorvaldsdóttir, H., Robinson, J. T., & Mesirov, J. P. (2013). Integrative Genomics Viewer (IGV): high-performance genomics data visualization and exploration. *Briefings in Bioinformatics*, *14*(2), 178-192. https://doi.org/10.1093/bib/bbs017

Villanueva, R. A. M., & Chen, Z. J. (2019). ggplot2: Elegant Graphics for Data Analysis, 2nd edition. *Measurement-Interdisciplinary Research and Perspectives*, *17*(3), 160-167. https://doi.org/10.1080/15366367.2019.1565254

Wang, X., Lu, Z. K., Gomez, A., Hon, G. C., Yue, Y. N., Han, D. L., Fu, Y., Parisien, M., Dai, Q., Jia, G.

1050 F., Ren, B., Pan, T., & He, C. (2014). *N*6-methyladenosine-dependent regulation of messenger
1051 RNA stability. *Nature*, *505*(7481), 117-120. https://doi.org/10.1038/nature12730
1052 Wang, Y., Li, Y., Toth, J. I., Petroski, M. D., Zhang, Z., & Zhao, J. C. (2014). *N*6-methyladenosine
1053 modification destabilizes developmental regulators in embryonic stem cells. *Nature Cell*
1054 *Biology*, *16*(2), 191-198. https://doi.org/10.1038/ncb2902
1055 Wang, Y., Li, Y., Yue, M. H., Wang, J., Kumar, S., Wechsler-Reya, R. J., Zhang, Z. L., Ogawa, Y., Kellis,
1056 M., Duester, G., & Zhao, J. C. (2018). N(6)-methyladenosine RNA modification regulates
1057 embryonic neural stem cell self-renewal through histone modifications. *Nature Neuroscience*,
1058 *21*(8), 1139-1139. https://doi.org/10.1038/s41593-018-0169-2
1059 Williams, B. R., Prabhu, V. R., Hunter, K. E., Glazier, C. M., Whittaker, C. A., Housman, D. E., &
1060 Amon, A. (2008). Aneuploidy affects proliferation and spontaneous immortalization in
1061 mammalian cells. *Science*, *322*(5902), 703-709. https://doi.org/10.1126/science.1160058
1062 Wu, T., Hu, E., Xu, S., Chen, M., Guo, P., Dai, Z., Feng, T., Zhou, L., Tang, W., Zhan, L., Fu, X., Liu, S.,
1063 Bo, X., & Yu, G. (2021). clusterProfiler 4.0: A universal enrichment tool for interpreting omics
1064 data. *Innovation (N Y)*, *2*(3), 100141. https://doi.org/10.1016/j.xinn.2021.100141
1065 Xie, W., & Birchler, J. A. (2012). Identification of Inverse Regulator-a (*Inr-a*) as Synonymous with
1066 Pre-mRNA Cleavage Complex II Protein (*Pcf11*) in *Drosophila*. *G3 (Bethesda)*, *2*(6), 701-706.
1067 https://doi.org/10.1534/g3.112.002071
1068 Yan, D., & Perrimon, N. (2015). *spenito* is required for sex determination in *Drosophila*
1069 *melanogaster*. *Proceedings of the National Academy of Sciences of the United States of*
1070 *America*, *112*(37), 11606-11611. https://doi.org/10.1073/pnas.1515891112
1071 Yang, H., Shi, X., Chen, C., Hou, J., Ji, T., Cheng, J., & Birchler, J. A. (2021). Predominantly inverse
1072 modulation of gene expression in genomically unbalanced disomic haploid maize. *Plant Cell*,
1073 *33*(4), 901-916. https://doi.org/10.1093/plcell/koab029
1074 Yang, Y., Hsu, P. J., Chen, Y. S., & Yang, Y. G. (2018). Dynamic transcriptomic m(6)A decoration:
1075 writers, erasers, readers and functions in RNA metabolism. *Cell Research*, *28*(6), 616-624.
1076 https://doi.org/10.1038/s41422-018-0040-8
1077 Yu, G. C., Wang, L. G., & He, Q. Y. (2015). ChIPseeker: an R/Bioconductor package for ChIP peak
1078 annotation, comparison and visualization. *Bioinformatics*, *31*(14), 2382-2383.
1079 https://doi.org/10.1093/bioinformatics/btv145

1080 Zaccara, S., Ries, R. J., & Jaffrey, S. R. (2019). Reading, writing and erasing mRNA methylation.
1081 *Nature Reviews: Molecular Cell Biology*, *20*(10), 608-624.
1082 https://doi.org/10.1038/s41580-019-0168-5
1083 Zhang, L. D., Zhang, S., Wang, R. X., & Sun, L. (2022). Genome-Wide Identification of Long
1084 Noncoding RNA and Their Potential Interactors in *ISWI* Mutants. *International Journal of*
1085 *Molecular Sciences*, *23*(11), 6247. https://doi.org/10.3390/ijms23116247
1086 Zhang, S., Qi, H., Huang, C., Yuan, L., Zhang, L., Wang, R., Tian, Y., & Sun, L. (2021a). Interaction of
1087 Male Specific Lethal complex and genomic imbalance on global gene expression in *Drosophila*.
1088 *Scientific Reports*, *11*(1), 19679. https://doi.org/10.1038/s41598-021-99268-y
1089 Zhang, S., Wang, R., Huang, C., Zhang, L., & Sun, L. (2021b). Modulation of Global Gene
1090 Expression by Aneuploidy and CNV of Dosage Sensitive Regulatory Genes. *Genes (Basel)*,
1091 *12*(10), 1606. https://doi.org/10.3390/genes12101606
1092 Zhang, S., Wang, R., Zhu, X., Zhang, L., Liu, X., & Sun, L. (2023). Characteristics and expression of
1093 lncRNA and transposable elements in *Drosophila* aneuploidy. *iScience*, *26*(12), 108494.
1094 https://doi.org/10.1016/j.isci.2023.108494
1095 Zhao, B. S., Wang, X., Beadell, A. V., Lu, Z., Shi, H., Kuuspalu, A., Ho, R. K., & He, C. (2017).
1096 m(6)A-dependent maternal mRNA clearance facilitates zebrafish maternal-to-zygotic
1097 transition. *Nature*, *542*(7642), 475-478. https://doi.org/10.1038/nature21355
1098 Zhong, S. L., Li, H. Y., Bodi, Z., Button, J., Vespa, L., Herzog, M., & Fray, R. G. (2008). MTA is an
1099 messenger RNA adenosine methylase and interacts with a homolog of a sex-specific splicing
1100 factor. *Plant Cell*, *20*(5), 1278-1288. https://doi.org/10.1105/tpc.108.058883
1101 Zhu, C., Zhang, S., Zhou, C., Tian, C., Shi, B., Xu, K., Huang, L., Sun, Y., Lin, Y., Lai, Z., & Guo, Y.
1102 (2023). RNA Methylome Reveals the m(6)A-mediated Regulation of Flavor Metabolites in Tea
1103 Leaves under Solar-withering. *Genomics Proteomics Bioinformatics*, *21*(4), 769-787.
1104 https://doi.org/10.1016/j.gpb.2023.02.003
1105
1106

1107 ## Figures

1108

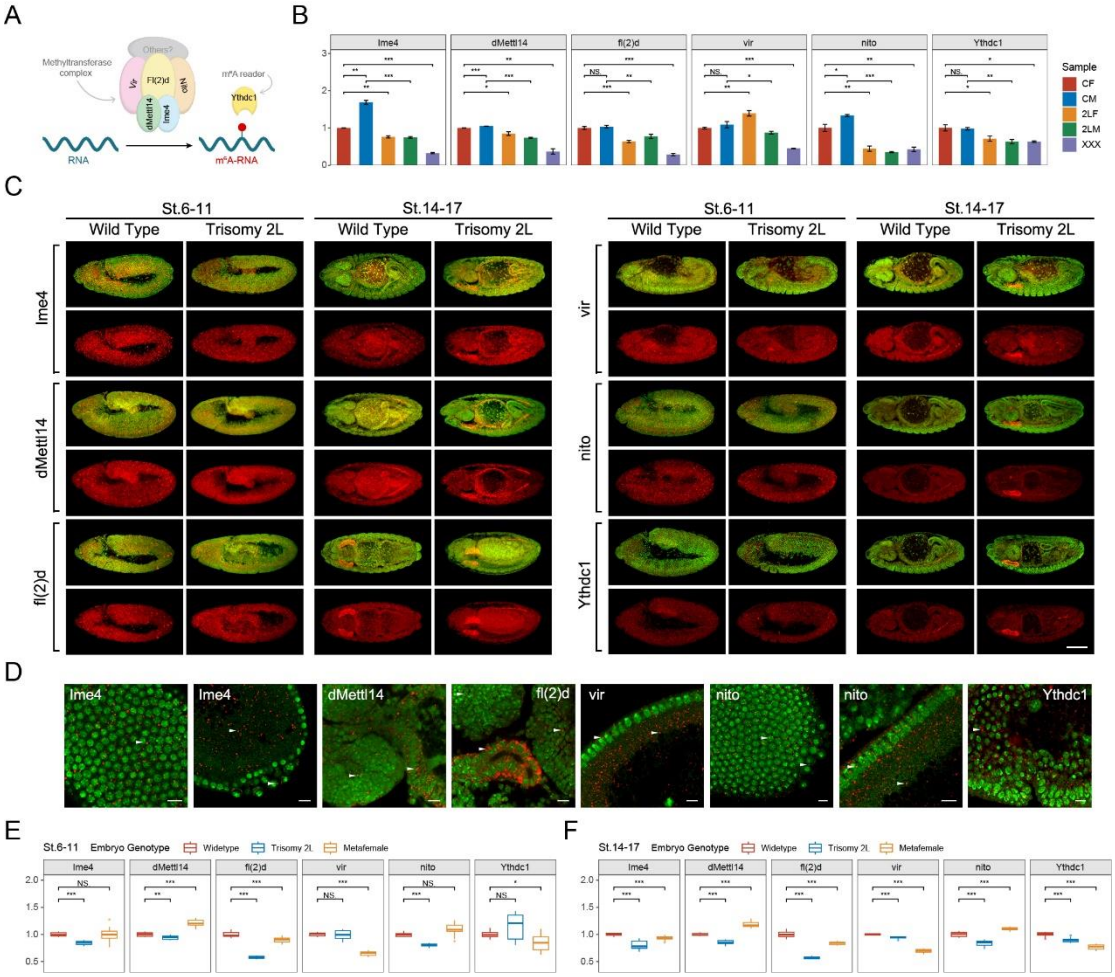

Figure 1. The responses of m^{6}A methyltransferases and reader protein under the condition of genomic imbalance. (**A**) Schematic diagram of m^{6}A components in *Drosophila*. (**B**) RT-qPCR analysis of mRNA levels of m^{6}A methyltransferases and reader protein in third instar larvae of wildtype and trisomy *Drosophila*. CF, wildtype female control; CM, wildtype male control; 2LF, trisomy 2L female; 2LM, trisomy 2L male; XXX, metafemale; 2L, chromosome 2 left arm. Student's *t* test *p < 0.05, **p < 0.01, ***p < 0.001. (**C**) Subembryonic distribution patterns of the transcripts of m^{6}A components in wildtype and trisomy 2L *Drosophila*. The names of the genes were shown in the left of the pictures; the genotypes and stages were shown above. Red, probes; green, DAPI. Scale bar, 100 µm. (**D**) Subcellular localization of probe signals. Probe name was written in the corner of each picture. Red, probe; green, DAPI. Arrowheads indicate the foci of probe signals. Scale bars, 10 µm. (**E**,**F**) The expression levels of m^{6}A component genes in stage 6-11 (**E**) and stage 14-17 (**F**) represented by relative fluorescence intensity of probes compared with DAPI signals. The expression of wildtype embryos was set as one. Sample size = 10. Student's *t* test *p < 0.05, **p < 0.01, ***p < 0.001.

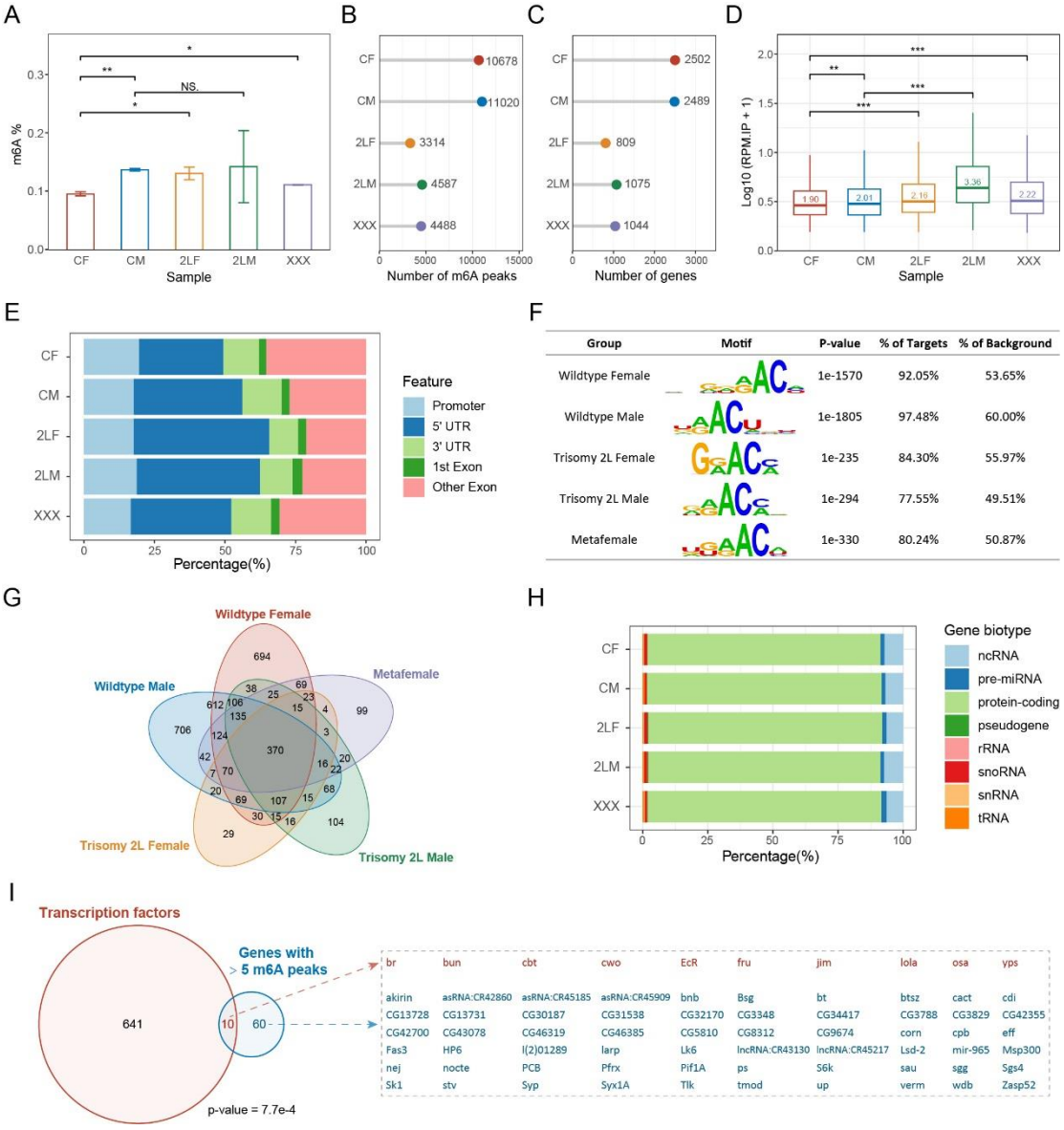

Figure 2. Overview of RNA m^{6}A methylation in aneuploid *Drosophila*. (**A**) Global m^{6}A abundance in third instar larvae of wildtype and aneuploid *Drosophila*. Data represent the mean of two independent experiments, each containing three or four biological replicates. Error bar indicates the standard error of the means (SEM). Student's *t* test *p < 0.05, **p < 0.01. (**B**) The number of m^{6}A peaks identified by MeRIP-Seq. (**C**) The number of m^{6}A-modified genes obtained by annotating the peaks. (**D**) Expression levels of m^{6}A modification sites in IP samples expressed as log10-transformed reads per million (RPM). The number on the boxplot indicates the median RPM of each sample. Mann-Whitney U test *p < 0.05, **p < 0.01, ***p < 0.001. (**E**) Percentages of peaks localized on different gene features. (**F**) The most enriched motifs obtained by *de novo*

motif analysis of the m^{6}A peaks. (**G**) Venn diagram showing the intersection of m^{6}A-modified genes in each sample. (**H**) Gene biotypes of m^{6}A-modified genes. (**I**) Venn diagram showing the intersection of transcription factors and m^{6}A-modified genes with more than five m^{6}A peaks in all samples. Seventy genes with more than five m^{6}A peaks were listed on the right, with transcription factors in red and others in blue. P-value indicates one-tailed Fisher's exact test. CF, wildtype female control; CM, wildtype male control; 2LF, trisomy 2L female; 2LM, trisomy 2L male; XXX, metafemale; 5'UTR, 5' untranslated region; 3'UTR, 3' untranslated region; MeRIP-Seq, m^{6}A methylated RNA immunoprecipitation sequencing.

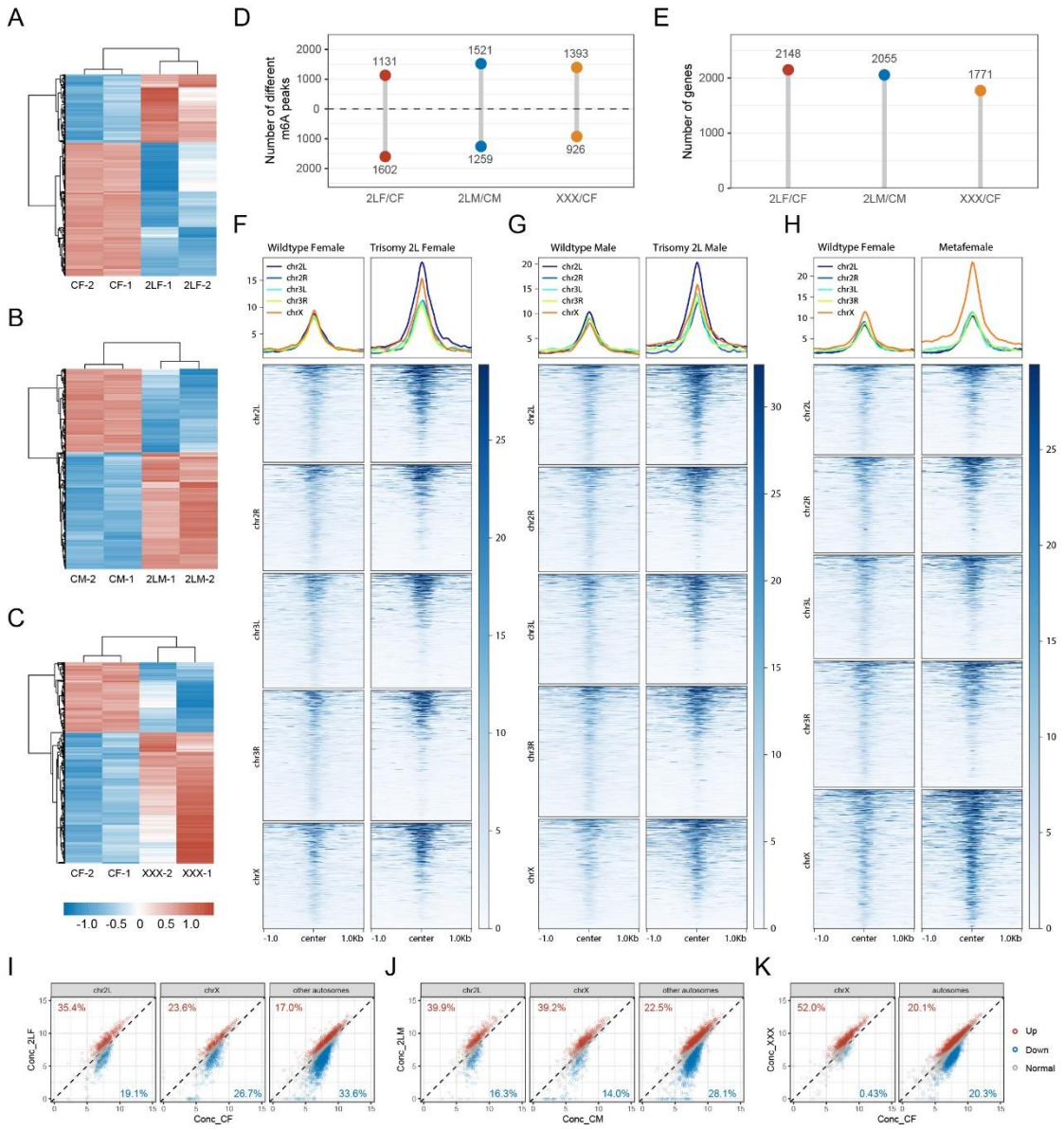

Figure 3. Differential m^{6}A methylome analysis of aneuploid *Drosophila*. (**A**-**C**) Heatmaps of

1146 differentially methylated peaks (DMPs) in trisomy 2L females (**A**), trisomy 2L males (**B**) and
1147 metafemales (**C**), and their corresponding control groups. The threshold of significance was
1148 p-value ≤ 0.1. (**D**) The number of DMPs. The threshold of significance was set to p-value ≤ 0.1.
1149 The numbers above the horizontal dashed lines indicate peaks with upregulated methylation
1150 levels, and the numbers below indicate peaks with downregulated methylation levels. (**E**) The
1151 number of DMP-associated genes. (**F**-**H**) Profiles and heatmaps illustrating the density of
1152 m^6A-modified reads at the DMP positions in trisomy 2L females (**F**), trisomy 2L males (**G**),
1153 metafemales (**H**), and their corresponding controls. The DMPs were divided into five groups
1154 according to the chromosomes they located. (**I**-**K**) Scatter plots showing the concentration of
1155 reads at methylation sites on different chromosomes in trisomy 2L females (**I**), trisomy 2L males
1156 (**J**), and metafemales (**K**). Red points indicate significantly up-regulated m^6A peaks, blue points
1157 indicate significantly down-regulated m^6A peaks, and gray points indicate m^6A peaks without
1158 significant changes. The percentages of DMPs on *cis* and *trans* chromosomes were indicated in
1159 the corners of the plots. CF, wildtype female control; CM, wildtype male control; 2LF, trisomy 2L
1160 female; 2LM, trisomy 2L male; XXX, metafemale.
1161

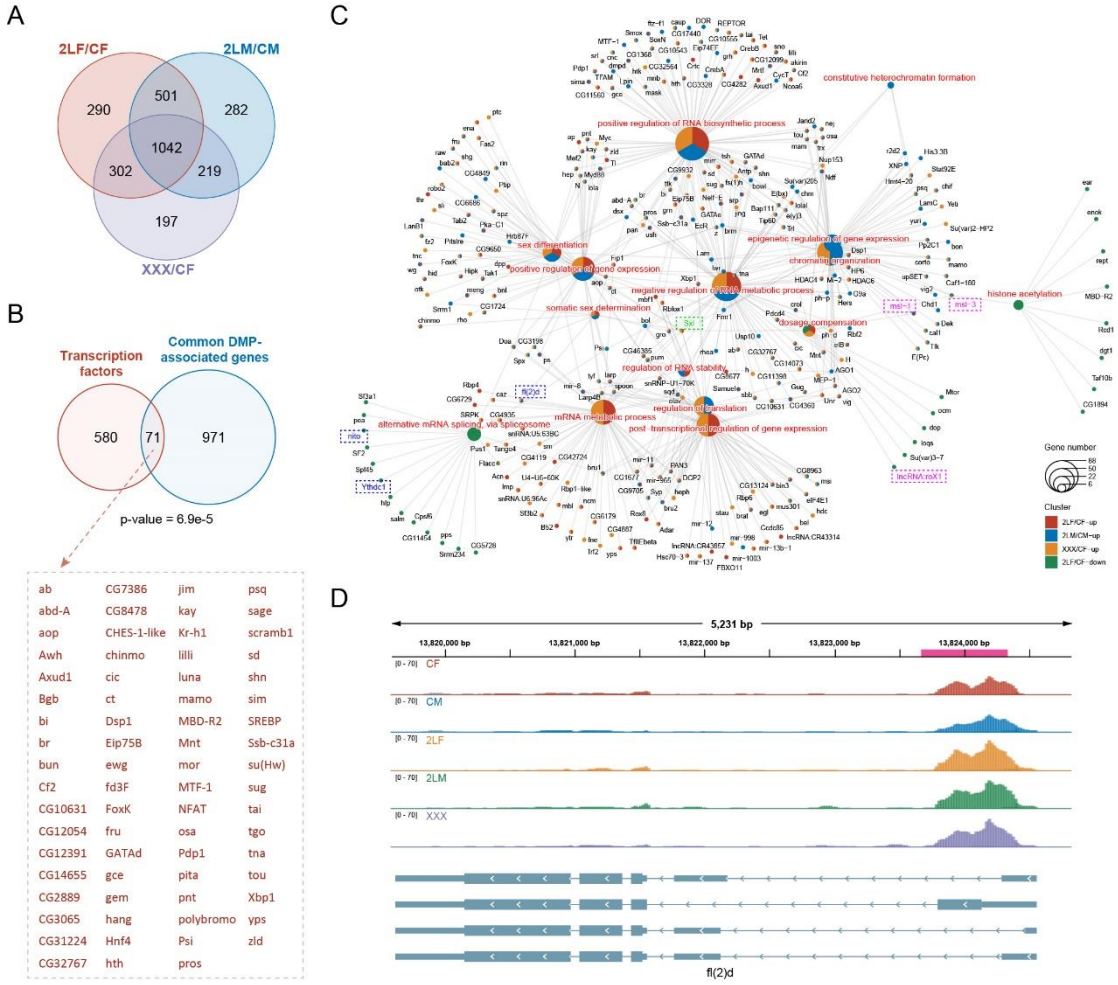

Figure 4. Differentially methylated peak (DMP) associated genes and their functions. (A) Venn diagram showing the number of common DMP-associated genes in three types of aneuploidies compared with wildtypes. (B) Venn diagram showing the intersection of transcription factors and the common DMP-associated genes in all comparisons. Transcription factors with DMPs were listed on the right. P-value indicates one-tailed Fisher's exact test. (C) Network showing the functions related to expression regulation and dosage compensation enriched by DMP-associated genes. The color of the nodes indicates the comparison, and the size of the function nodes represents the number of DMP-associated genes connected with them. (D) Genome browser example of *fl(2)d* for indicated MeRIP-seq data. Steelblue color represents input reads, while other colors represent IP reads. Signals were displayed as the mean CPM of two biological replicates. The gene architectures were shown at the bottom. The magenta rectangles at above represent differentially methylated peak. CF, wildtype female control; CM, wildtype male control; 2LF, trisomy 2L female; 2LM, trisomy 2L male; XXX, metafemale.

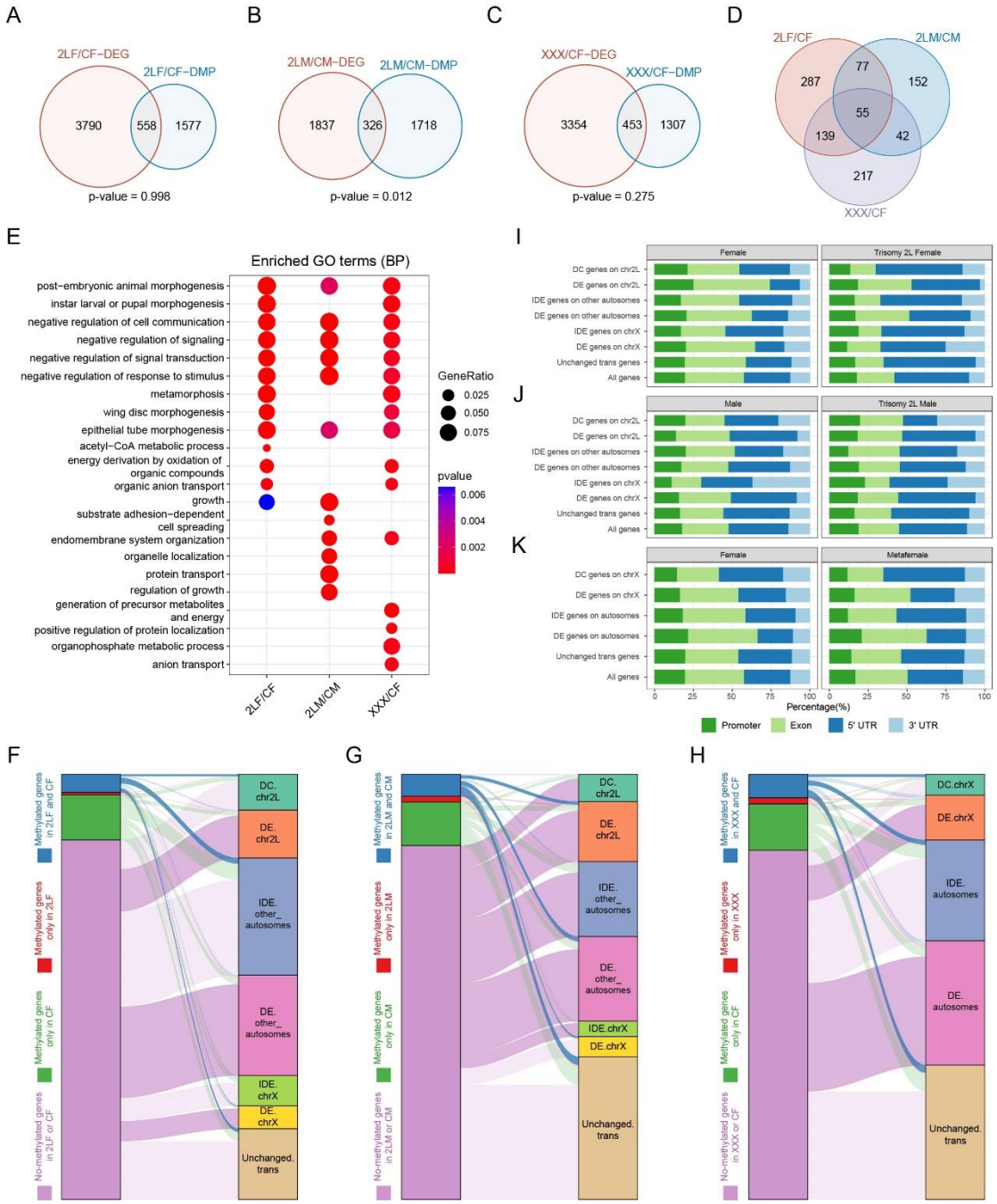

Figure 5. Relationships between RNA m^{6}A methylation and gene expression in aneuploidy. (**A**-**C**) Venn diagrams showing the intersections of differentially expressed genes (DEGs) and differentially methylated peak (DMP) associated genes in trisomy 2L females (**A**), trisomy 2L males (**B**), and metafemales (**C**) compared with their corresponding controls. P-values indicate one-tailed Fisher's exact tests. (**D**) The common differentially expressed and differentially methylated genes in all groups. (**E**) Functional enrichment analysis of simultaneously differentially expressed and differentially methylated genes. Top 10 enriched GO terms (Biological Process) with p-value < 0.1 in each comparison were shown. (**F**-**H**) Sankey diagrams showing the

1186 relationships between genes with different m^6A-modified states and genes with canonical dosage
1187 effect (DE), dosage compensation (DC), and inverse dosage effect (IDE) in trisomy 2L females (**F**),
1188 trisomy 2L males (**G**), and metafemales (**H**). Enrichment analysis was performed on each two
1189 groups of genes, and deep color lines indicate significant connection relationships (Fisher's exact
1190 test p-value < 0.05). (**I**-**K**) Gene feature distributions for m^6A peaks on genes with canonical DE,
1191 DC, and IDE in trisomy 2L females (**I**), trisomy 2L males (**J**), metafemales (**K**), and their
1192 corresponding controls. CF, wildtype female control; CM, wildtype male control; 2LF, trisomy 2L
1193 female; 2LM, trisomy 2L male; XXX, metafemale; DEG, differentially expressed gene; DMP,
1194 differentially methylated peak; DE, dosage effect; DC, dosage compensation; IDE, inverse dosage
1195 effect. Canonical DE refers to ratio > 1.25, DC stands for 0.8 < ratio < 1.25, IDE stands for 0.5 <
1196 ratio < 0.8, and unchanged refers to 0.8 < ratio < 1.25.
1197

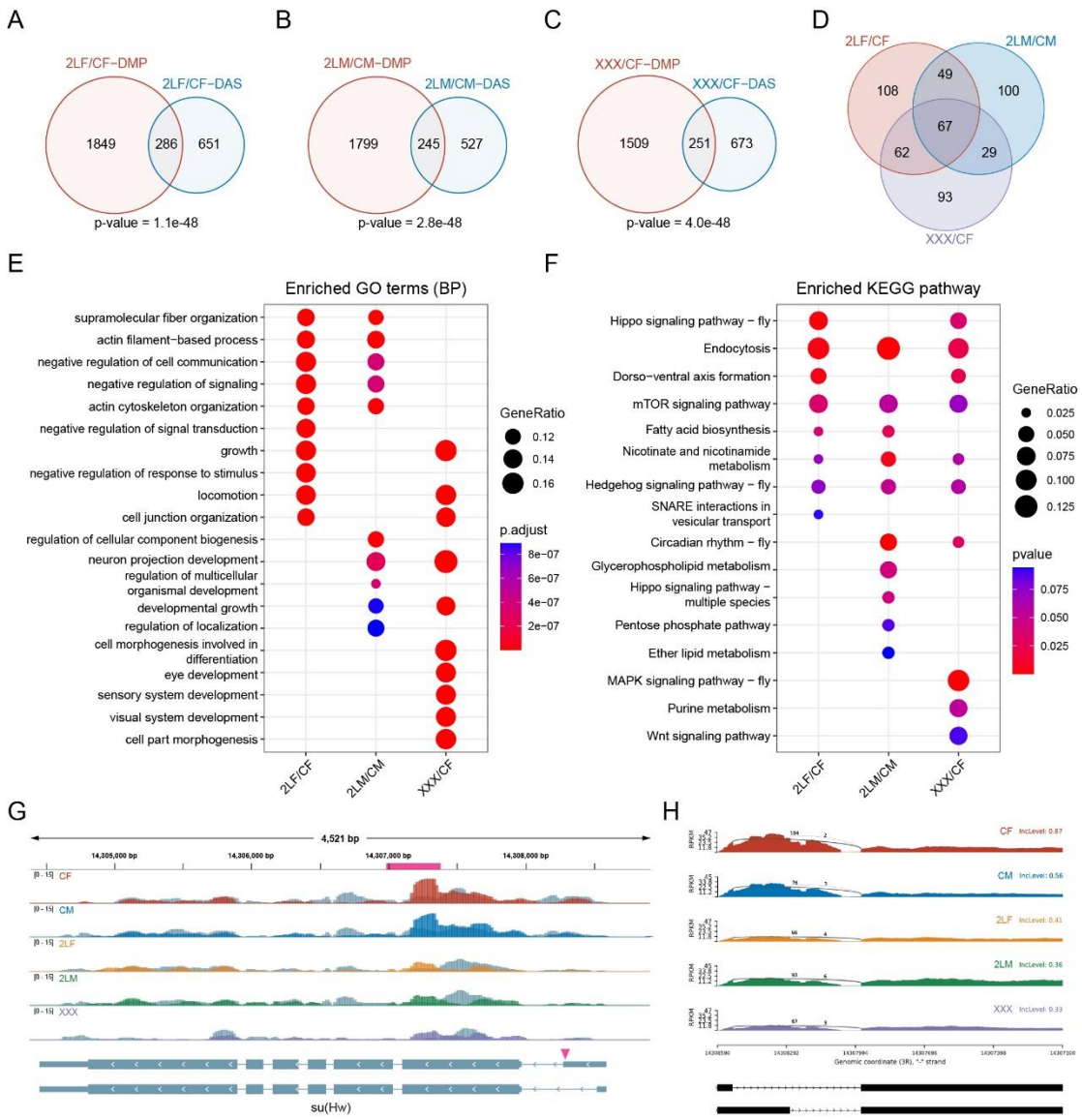

Figure 6. Combined analysis of differential alternative splicing and differential methylation. (**A**-**C**) Venn diagrams showing the intersections of differential alternative splicing (DAS) genes and differentially methylated peak (DMP) associated genes in trisomy 2L females (**A**), trisomy 2L males (**B**), and metafemales (**C**) compared with their corresponding controls. P-values indicate one-tailed Fisher's exact tests. (**D**) The common differentially alternatively spliced and differentially methylated genes in all groups. (**E**) Functional enrichment analysis of simultaneously differentially alternatively spliced and differentially methylated genes. Top 10 enriched GO terms (Biological Process) with p-value < 0.05 in each comparison were shown. (**F**) KEGG pathway enrichment analysis of simultaneously differentially alternatively spliced and differentially methylated genes. Top 10 enriched pathways with p-value < 0.1 in each comparison were shown. (**G**) Genome browser example of *su(Hw)* for indicated MeRIP-Seq data. Steelblue color represents

input reads, while other colors represent IP reads. Signals were displayed as the mean CPM of two biological replicates. The gene architecture was shown at the bottom (only two representative transcript isoforms were shown). The magenta rectangle at above represents DMP. The magenta arrowhead indicates the position of differential alternative splicing. (**H**) Sashimi plot depicting RNA sequencing reads and exon junction reads at the position where the differential splicing events occurs on *su(Hw)*. The gene model was shown below. One of the biological replicates was chosen for representation. CF, wildtype female control; CM, wildtype male control; 2LF, trisomy 2L female; 2LM, trisomy 2L male; XXX, metafemale; DAS, differential alternative splicing; DMP, differentially methylated peak; CPM, Counts per million; RPKM, Reads per kilobase per million mapped reads.

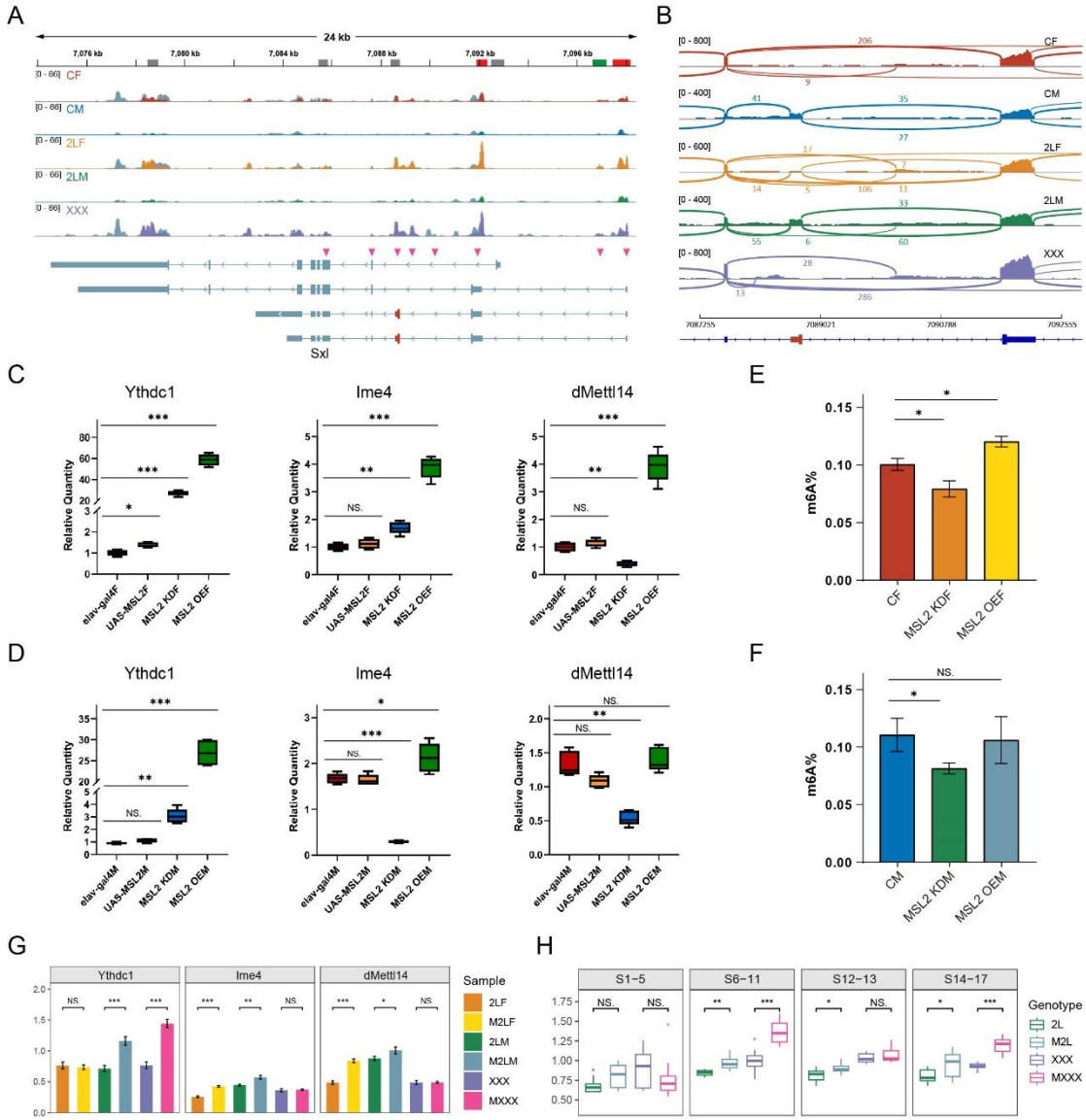

1222 **Figure 7.** Interactions between m^6A and *Drosophila* Male Specific Lethal (MSL) complex. (**A**)
1223 Genome browser example of *Sxl* for indicated MeRIP-Seq data. Steelblue color represents input
1224 reads, while other colors represent IP reads. Signals were displayed as the mean CPM of two
1225 biological replicates. The gene architecture was shown at the bottom (only four representative
1226 transcript isoforms were shown). The rectangles at above represent m^6A peaks, where red
1227 indicates up-regulated DMPs, green indicates down-regulated DMP, and gray indicates no
1228 significant changes. The magenta arrowheads indicate the positions of alternative splicing. (**B**)
1229 Sashimi plot depicting RNA sequencing reads and exon junction reads at the position where the
1230 differential splicing events occurs on *Sxl*. The gene model was shown below, with the third exon
1231 indicated in red. One of the biological replicates was chosen for representation. CF, wildtype
1232 female control; CM, wildtype male control; 2LF, trisomy 2L female; 2LM, trisomy 2L male; XXX,
1233 metafemale. (**C,D**) RT-qPCR analysis of mRNA levels of m^6A components in the heads of MSL2
1234 transgenic female (**C**) and male (**D**) *Drosophila* adults. (**E**,**F**) Abundance of m^6A modification in the
1235 heads of MSL2 transgenic females (**E**) and males (**F**). Student's *t* test *p < 0.05, **p < 0.01, ***p <
1236 0.001. MSL2 KDF, MSL2 neural-knockdown female; MSL2 KDM, MSL2 neural-knockdown male;
1237 MSL2 OEF, MSL2-overexpressed female; MSL2 OEM, MSL2-overexpressed male. (**G**) RT-qPCR
1238 analysis of mRNA levels of m^6A regulators in the brains of trisomy and MSL2-overexpressed
1239 trisomy *Drosophila* larvae. Student's *t* test *p < 0.05, **p < 0.01, ***p < 0.001. 2LF, trisomy 2L
1240 female; 2LM, trisomy 2L male; XXX, metafemale; M2LF, MSL2-overexpressed trisomy 2L female;
1241 M2LM, MSL2-overexpressed trisomy 2L male; MXXX, MSL2-overexpressed metafemale. (**H**) The
1242 expression levels of Ime4 in trisomy and MSL2-overexpressed trisomy embryos represented by
1243 relative fluorescence intensity of probes. The expression of wildtype embryos was set as one.
1244 Sample size = 10. Student's *t* test *p < 0.05, **p < 0.01, ***p < 0.001. 2L, trisomy 2L; M2L,
1245 MSL2-overexpressed trisomy 2L; XXX, metafemale; MXXX, MSL2-overexpressed metafemale.
1246

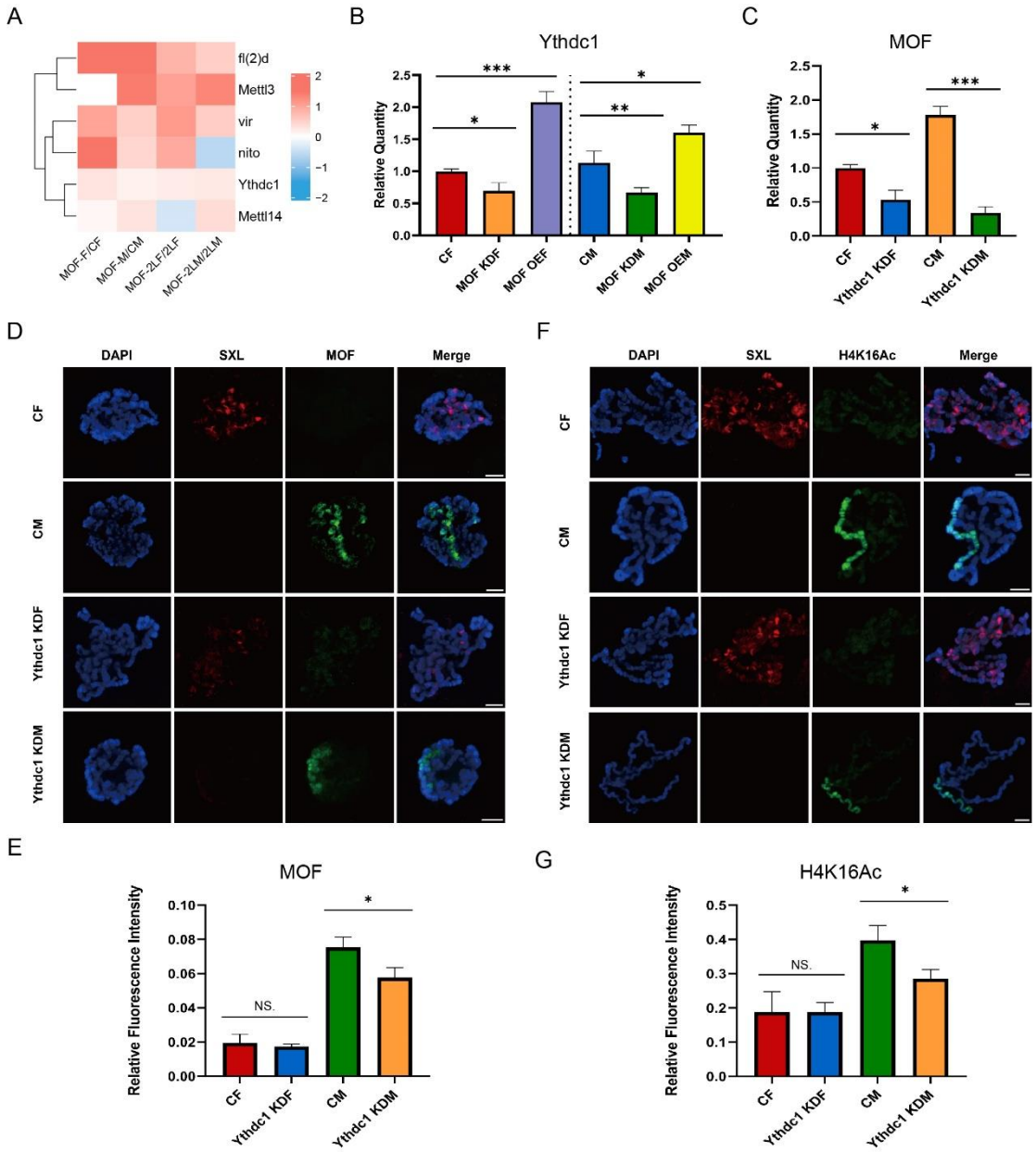

Figure 8. RNA m^{6}A modification may regulate H4K16Ac through histone acetyltransferase MOF. (**A**) Heatmap of the expression changes of m^{6}A regulators in MOF overexpressing *Drosophila* larvae. The color of the heatmap represents log2(ratio). CF, wildtype female control; CM, wildtype male control; MOF-F, MOF-overexpressed female; MOF-M, MOF-overexpressed male; 2LF, trisomy 2L female; 2LM, trisomy 2L male; MOF-2LF, MOF-overexpressed trisomy 2L female; MOF-2LM, MOF-overexpressed trisomy 2L male. (**B**) RT-qPCR analysis of mRNA levels of Ythdc1 in the heads of MSL2 transgenic *Drosophila.* (**C**) RT-qPCR analysis of mRNA levels of MOF in the heads of *Ythdc1* knockdown *Drosophila*. (**D**) Immunofluorescence of polytene chromosomes showed the signals of SXL (red channel) and MOF (green channel) in the salivary glands of

1257 *Drosophila* larvae of different genotypes. (**E**) The levels of MOF in the salivary glands of *Ythdc1*
1258 knockdown *Drosophila* quantified by immunofluorescence. (**F**) Immunofluorescence of polytene
1259 chromosomes showed the signals of SXL (red channel) and H4K16Ac (green channel) in the
1260 salivary glands of *Drosophila* larvae of different genotypes. (**G**) The levels of H4K16Ac in the
1261 salivary glands of *Ythdc1* knockdown *Drosophila* quantified by immunofluorescence. Scale bars,
1262 10 µm. Student's *t* test *p < 0.05, **p < 0.01, ***p < 0.001. CF, wildtype female control; CM,
1263 wildtype male control; MOF KDF, MOF neural-knockdown female; MOF KDM, MOF
1264 neural-knockdown male; MOF OEF, MOF-overexpressed female; MOF OEM, MOF-overexpressed
1265 male; Ythdc1 KDF, Ythdc1-knockdown female; Ythdc1 KDM, Ythdc1-knockdown male; Ythdc1 OEF,
1266 Ythdc1-overexpressed female; Ythdc1 OEM, Ythdc1-overexpressed male.
1267
1268

1269 ## Figure supplements

1270

A

Primer	Sequence	Length
Ime4-L	CAAGTACGTGCACTATGAGG	159
Ime4-R	GTCATGTCCAAGAAGCGTAG	
dMettl14-L	GCCTCTTCCTCCAAGAAAAC	189
dMettl14-R	CCTCAACTTGGGATACTCCT	
fl(2)d-L	CCTGGACGTTATTTCCTACT	245
fl(2)d-R	TAAGCTAGAGACCATTCACG	
vir-L	GTACATGAAACCCTTAGAGGC	154
vir-R	CTTGCTTATGGAGAGATAGCG	
nito-L	GCCAGTACGGTTCCAGATGT	104
nito-R	CCGTCCGTCAAATGAAACTT	
Ythdc1-L	GGTCGTGATTTGATCCTCTG	153
Ythdc1-R	TCGAACTCACTCCCATACTC	
tubulin-F	AGCTCAGCACCCTCTGTGTAAT	208
tubulin-R	AGCTGGAGCGCATCAATGTGTA	

B

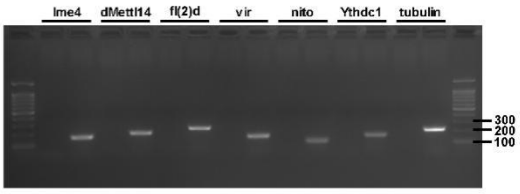

C

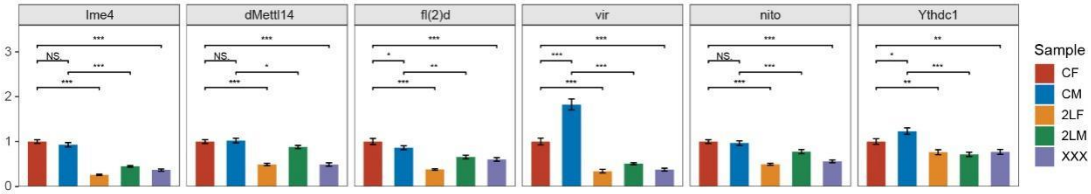

D

Primer	Sequence	Length
Ime4-F-T3	TGTTGGGAAATCACTCCCAATTAAGAGAAGTTTAAGTCCCACGG	1126
Ime4-R-T7	GTAATACGACTCACTATAGGGAGACCACCATCTGGATAACGCTTCTGG	
dMettl14-F-T3	TGTTGGGAAATCACTCCCAATTAACCAATCCGCACAATGACTAC	752
dMettl14-R-T7	GTAATACGACTCACTATAGGGAGACCACTAGCCAACCTGGTCGAATAC	
fl(2)d-F-T3	TGTTGGGAAATCACTCCCAATTAACTAGAGACCATTCACGAGGA	829
fl(2)d-R-T7	GTAATACGACTCACTATAGGGAGACCACATTATGTATGTCTACGCCGC	
vir-F-T3	TGTTGGGAAATCACTCCCAATTAACGAAATGTCGTACAAGGTGC	530
vir-R-T7	GTAATACGACTCACTATAGGGAGACCACGATCTCCGGGAAAAGTGGTT	
nito-F-T3	TGTTGGGAAATCACTCCCAATTAACTCCGATTGATCCCTACGAT	1324
nito-R-T7	GTAATACGACTCACTATAGGGAGACCACGTATCTCCGTCCGTCAAATG	
Ythdc1-F-T3	TGTTGGGAAATCACTCCCAATTAACGAATCGAATGGTGGAGACT	622
Ythdc1-R-T7	GTAATACGACTCACTATAGGGAGACCACCCGTGTGTCTCGGAATAGGT	

E

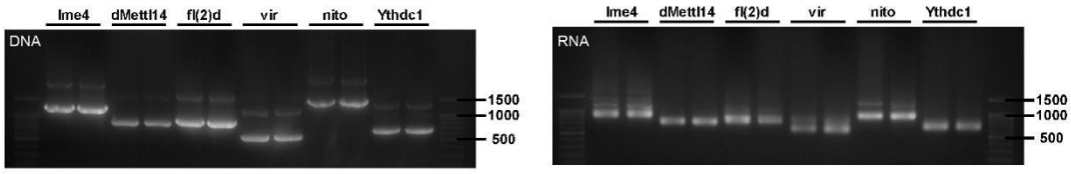

Figure 1—figure supplement 1. Primers of m^{6}A methyltransferases and reader protein for RT-qPCR and TSA-FISH. (**A**) The sequences of RT-qPCR primers. (**B**) Agarose gel electrophoresis validation of qPCR primers. The left lane of each gene is negative control with primers only and no DNA substrate. (**C**) RT-qPCR analysis of mRNA levels of m^{6}A methyltransferases and reader protein in the brains of wildtype and trisomy *Drosophila* larvae. CF, wildtype female control; CM, wildtype male control; 2LF, trisomy 2L female; 2LM, trisomy 2L male; XXX, metafemale. Student's *t* test *p < 0.05, **p < 0.01, ***p < 0.001. (**D**) The sequences of FISH primers. (**E**) The sizes of the products of the FISH primers after PCR amplification and in vitro transcription were tested by agarose gel electrophoresis. 2L, chromosome 2 left arm; RT-qPCR, Real-time quantitative PCR; TSA-FISH, Tyramide signal amplification-based fluorescence *in situ* hybridization.

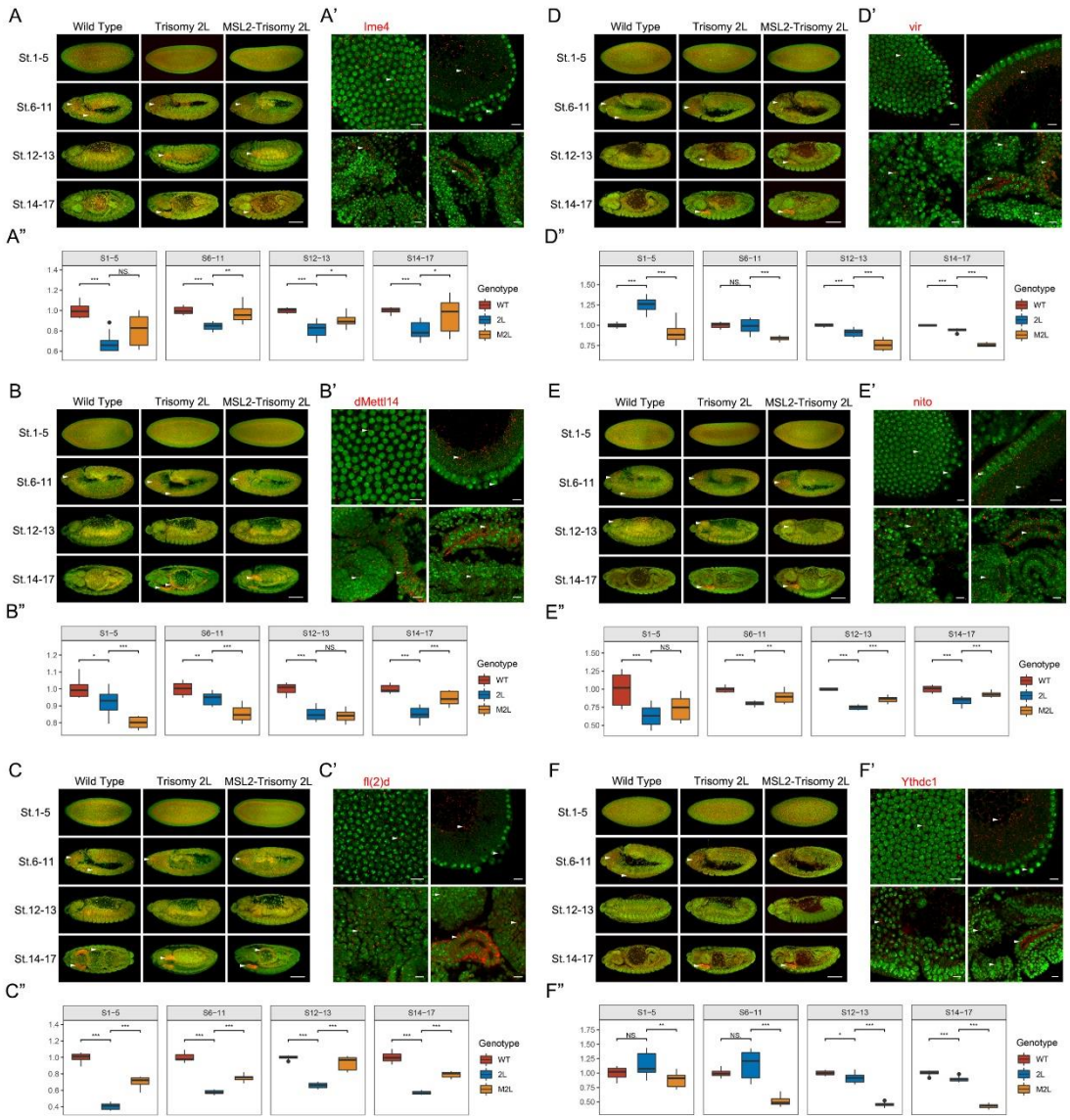

Figure 1—figure supplement 2. Embryo TSA-FISH of m^{6}A components in wildtype, trisomy, and MSL2-overexpressed trisomy *Drosophila*. The images represent m^{6}A component *Ime4* (**A-A"**), *dMettl14* (**B-B"**), *fl(2)d* (**C-C"**), *vir* (**D-D"**), *nito* (**E-E"**), and *Ythdc1* (**F-F"**), respectively. (**A-F**) Gene expression patterns in entire embryos. The genotypes of the samples were shown above, and the development stages (St.) were shown in the left of the pictures. The red pseudocolor represents signal from the probes, and green is the signal of nucleus. Arrowheads indicate regions where the probe signal are enriched. Scale bars, 100 µm. (**A'-F'**) RNA subcellular location patterns of m^{6}A components. Arrowheads indicate probe signals. Scale bars, 10 µm. (**A"-F"**) The expression levels of m^{6}A component genes represented as relative fluorescence intensity of the probes compared with DAPI. The expression of wildtype embryos was set as base line. WT, wildtype; 2L, trisomy 2L; M2L, MSL2-overexpressed trisomy 2L. Sample size = 10. Student's *t* test *p < 0.05, **p < 0.01,

***p < 0.001.

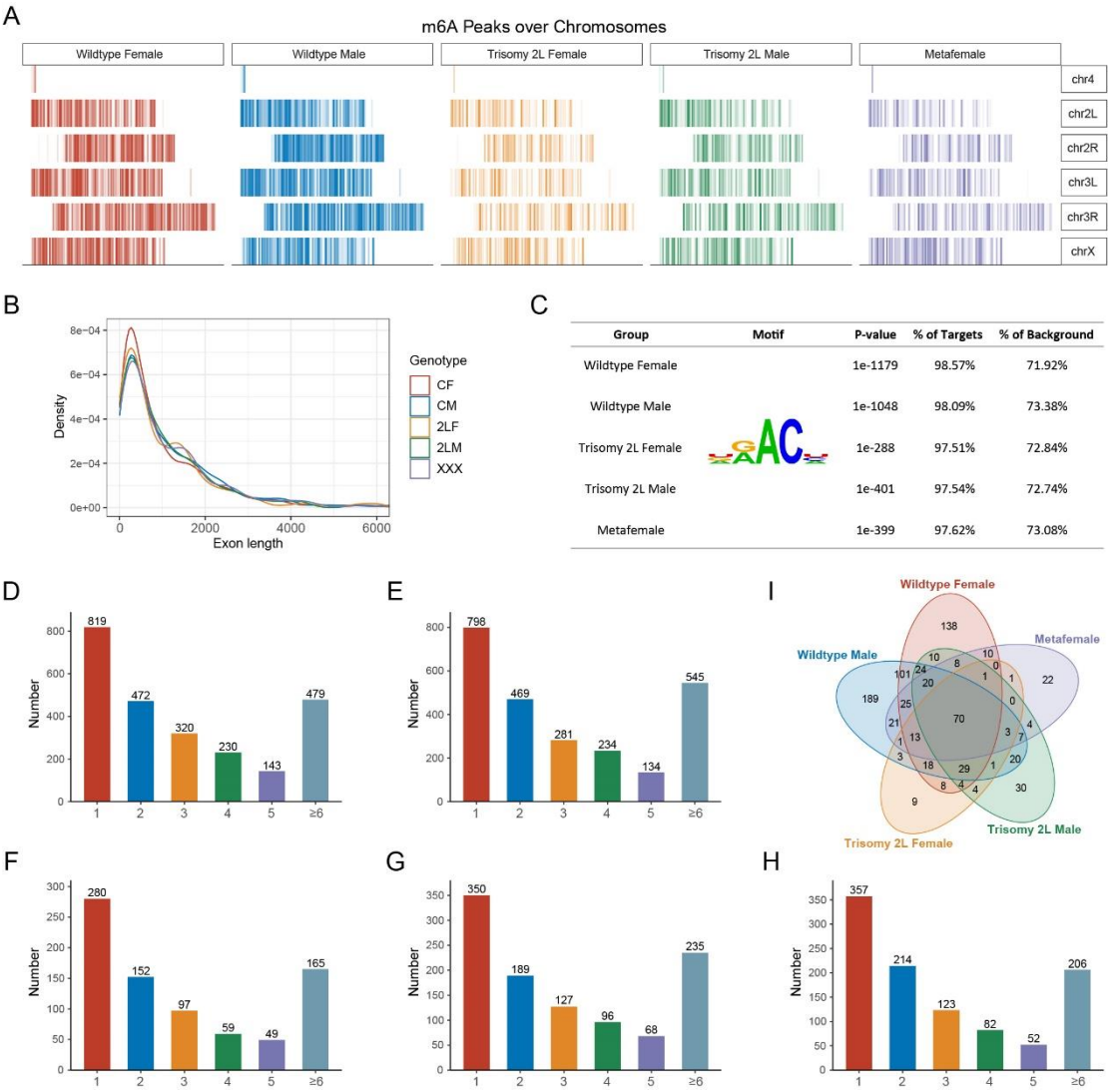

Figure 2—figure supplement 1. Characteristics of m^{6}A-modified genes in wildtype and aneuploid *Drosophila*. (**A**) Distribution of m^{6}A peaks along each chromosome. (**B**) Kernel density plot showing the distribution of exon lengths of m^{6}A-modified genes. CF, wildtype female control; CM, wildtype male control; 2LF, trisomy 2L female; 2LM, trisomy 2L male; XXX, metafemale. (**C**) Enrichment analysis performed on the known m^{6}A consensus motif DRACH (D = G/A/U, R = G/A, H = U/A/C). (**D**-**H**) Statistics of the number of m^{6}A peaks on m^{6}A-modified genes in wildtype females (**D**), wildtype males (**E**), trisomy 2L females (**F**), trisomy 2L males (**G**), and metafemales (**H**). (**I**) Venn diagram showing the number of m^{6}A-modified genes with more than five m^{6}A peaks.

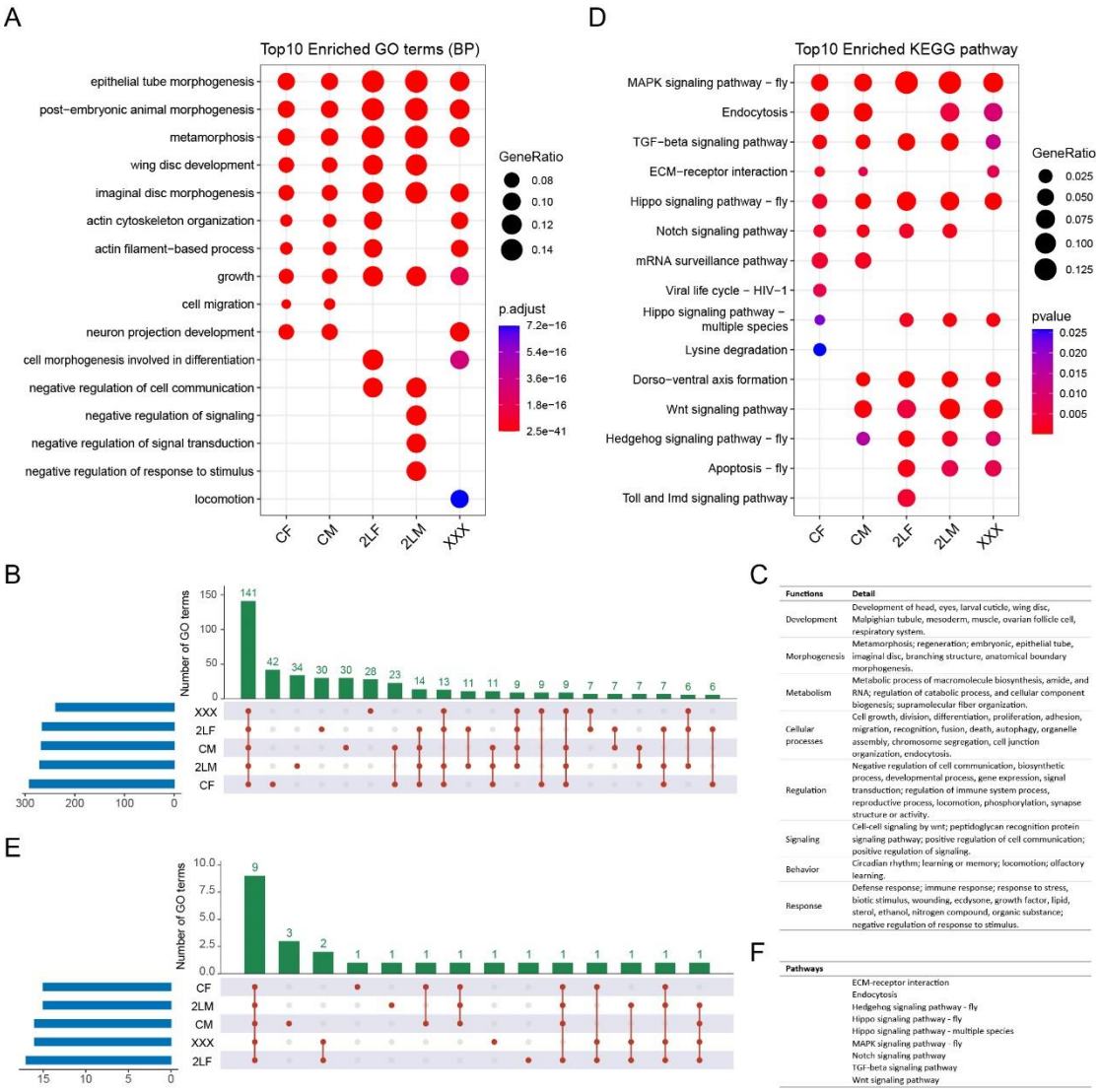

Figure 2—figure supplement 2. Functional and pathway analysis of m^{6}A-modified genes in wildtype and aneuploid *Drosophila*. (**A**) Functional enrichment analysis of m^{6}A-modified genes. Top 10 enriched GO terms (Biological Process) with adjusted p-value < 0.05 in each sample were shown. (**B**) UpSet plot showing the shared sets of enriched GO terms of m^{6}A-modified genes in different groups. (**C**) Summary of the common functions enriched by m^{6}A-modified genes in all genotypes. (**D**) KEGG pathway enrichment analysis of m^{6}A-modified genes. Top 10 enriched pathways with p-value < 0.05 in each sample were shown. (**E**) UpSet plot showing the shared sets of enriched KEGG pathways of m^{6}A-modified genes in different groups. (**F**) The pathways enriched in all genotypes were listed. CF, wildtype female control; CM, wildtype male control; 2LF, trisomy 2L female; 2LM, trisomy 2L male; XXX, metafemale; GO, Gene Ontology; BP, Biological Process; KEGG, Kyoto Encyclopedia of Genes and Genomes.

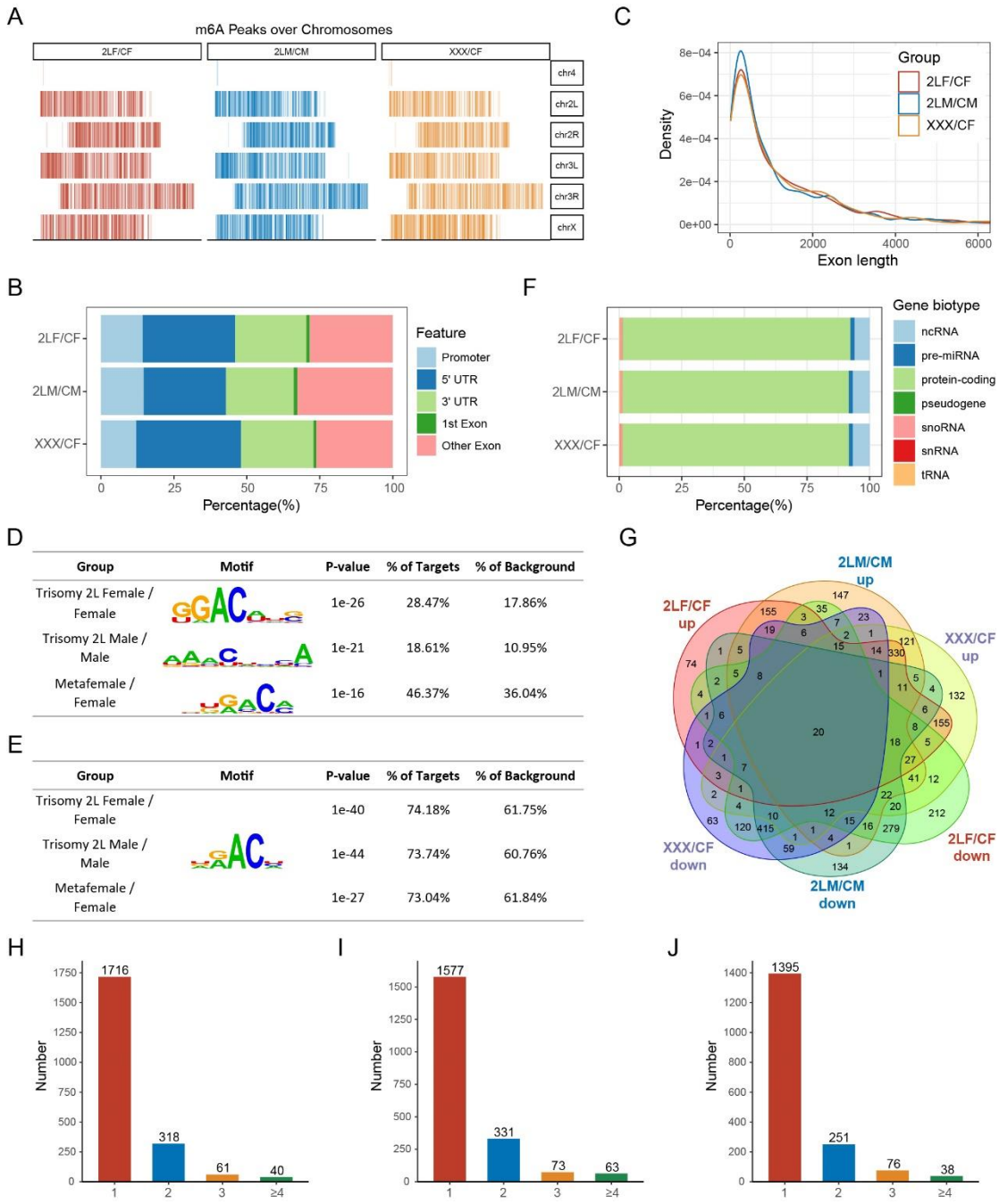

Group	Motif	P-value	% of Targets	% of Background
Trisomy 2L Female / Female		1e-26	28.47%	17.86%
Trisomy 2L Male / Male		1e-21	18.61%	10.95%
Metafemale / Female		1e-16	46.37%	36.04%

Group	Motif	P-value	% of Targets	% of Background
Trisomy 2L Female / Female		1e-40	74.18%	61.75%
Trisomy 2L Male / Male		1e-44	73.74%	60.76%
Metafemale / Female		1e-27	73.04%	61.84%

Figure 3—figure supplement 1. Characteristics of differentially methylated peak (DMP) associated genes. (**A**) Distribution of differentially methylated peaks (DMPs) along each chromosome. (**B**) Percentages of DMPs localized on different gene features. (**C**) Kernel density plot showing the distribution of exon lengths of DMP-associated genes. (**D**) The top enriched motifs with *de novo* motif analysis of DMPs in each comparison. (**E**) Enrichment analysis performed on the known m^6A consensus motif DRACH (D = G/A/U, R = G/A, H = U/A/C). (**F**) Gene biotypes of DMP-associated genes. (**G**) Venn diagram showing the intersection of DMP-associated genes in each comparison. (**H-J**) Statistics of the number of DMPs on DMP-associated genes in

trisomy 2L females compared with wildtype females (**H**), trisomy 2L males compared with wildtype males (**I**), and metafemales compared with wildtype females (**J**). CF, wildtype female control; CM, wildtype male control; 2LF, trisomy 2L female; 2LM, trisomy 2L male; XXX, metafemale; 5'UTR, 5' untranslated region; 3'UTR, 3' untranslated region.

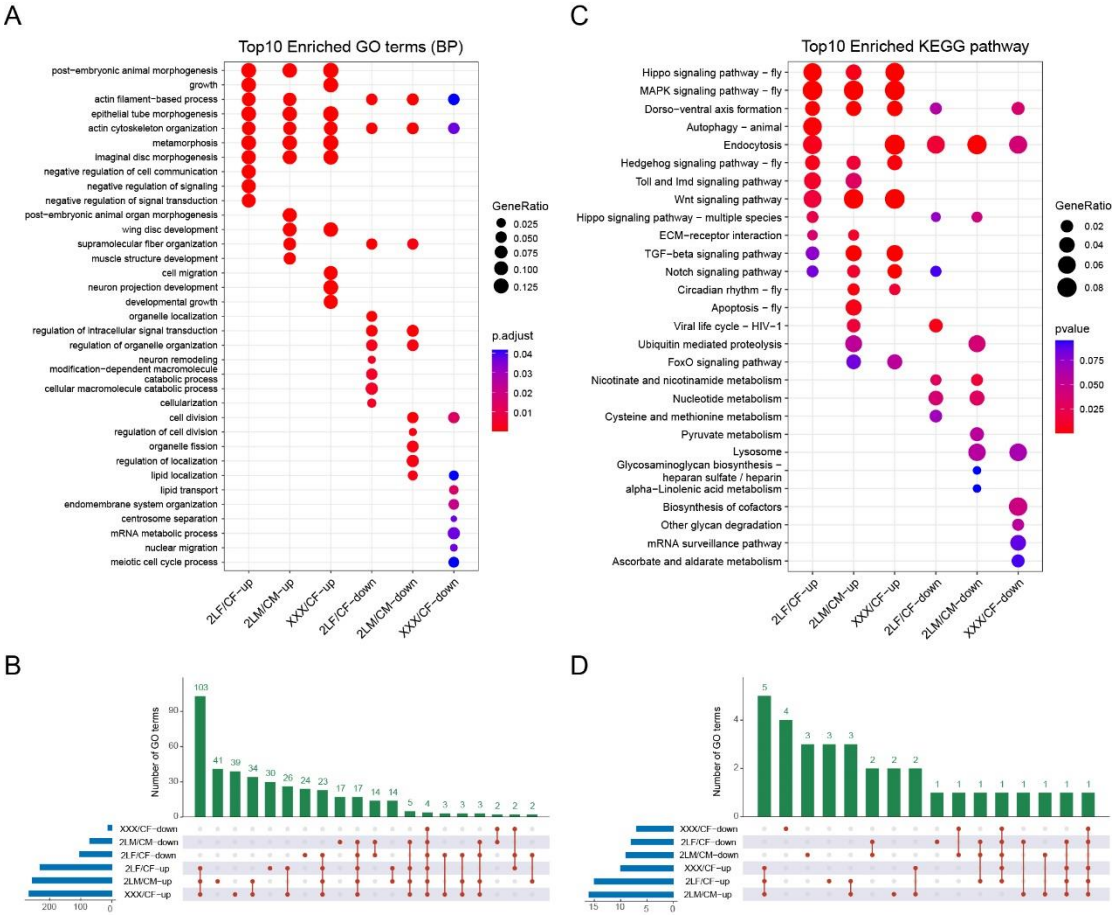

Figure 4—figure supplement 1. Functional and pathway analysis of DMP-associated genes. (**A**) Functional enrichment analysis of DMP-associated genes. Top 10 enriched GO terms (Biological Process) with adjusted p-value < 0.05 in each comparison were shown. (**B**) UpSet plot showing the shared sets of enriched GO terms of DMP-associated genes in different aneuploidies. (**C**) KEGG pathway enrichment analysis of DMP-associated genes. Top 10 enriched pathways with p-value < 0.1 in each comparison were shown. (**D**) UpSet plot showing the shared sets of enriched KEGG pathways of DMP-associated genes in different aneuploidies. CF, wildtype female control; CM, wildtype male control; 2LF, trisomy 2L female; 2LM, trisomy 2L male; XXX, metafemale.

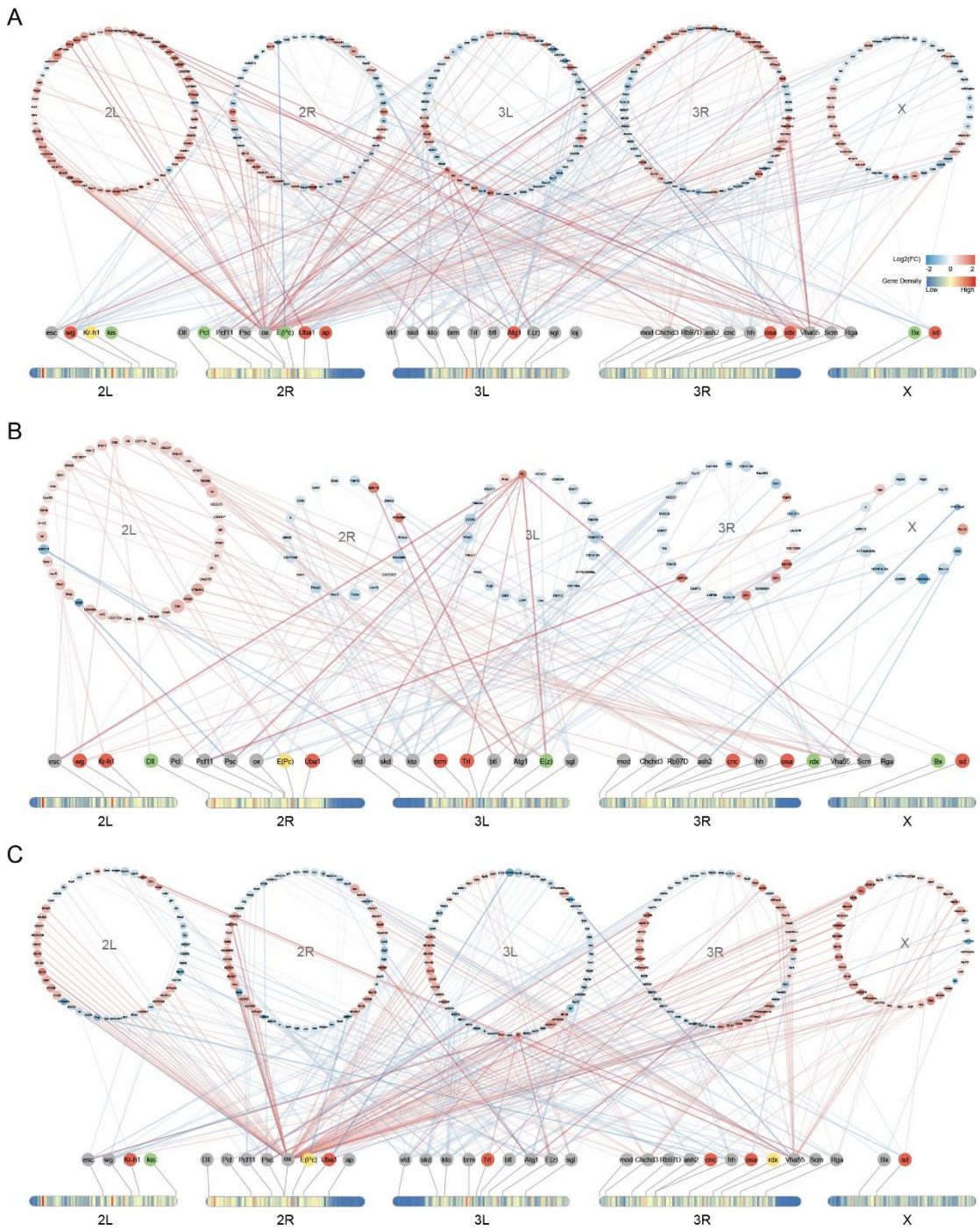

Figure 5—figure supplement 1. Dosage-sensitive modifiers and their interactors in aneuploid *Drosophila*. (**A**-**C**) Networks showing the methylation status of known dosage-sensitive modifiers and the expression changes of genes interact with these modifiers in trisomy 2L females (**A**), trisomy 2L males (**B**), and metafemales (**C**), respectively. Protein-protein interaction (PPI) relationships were obtained from the STRING database. The colors of the heatmaps on chromosomes represent the gene density. Dosage-sensitive modifiers were arranged according to their localizations, with red indicating genes with upregulated DMPs, green indicating genes with

1354 downregulated DMPs, yellow indicating genes with both up- and down-regulated DMPs, and grey
1355 indicating genes without DMPs. The interactors of these modifiers were also separated by
1356 chromosomes, and the colors of the nodes and edges indicate the log2(fold changes) of gene
1357 expression in trisomies. The width of the edges represents the combined score, and only
1358 interactions with combined score ≥ 700 were selected for presentation.
1359

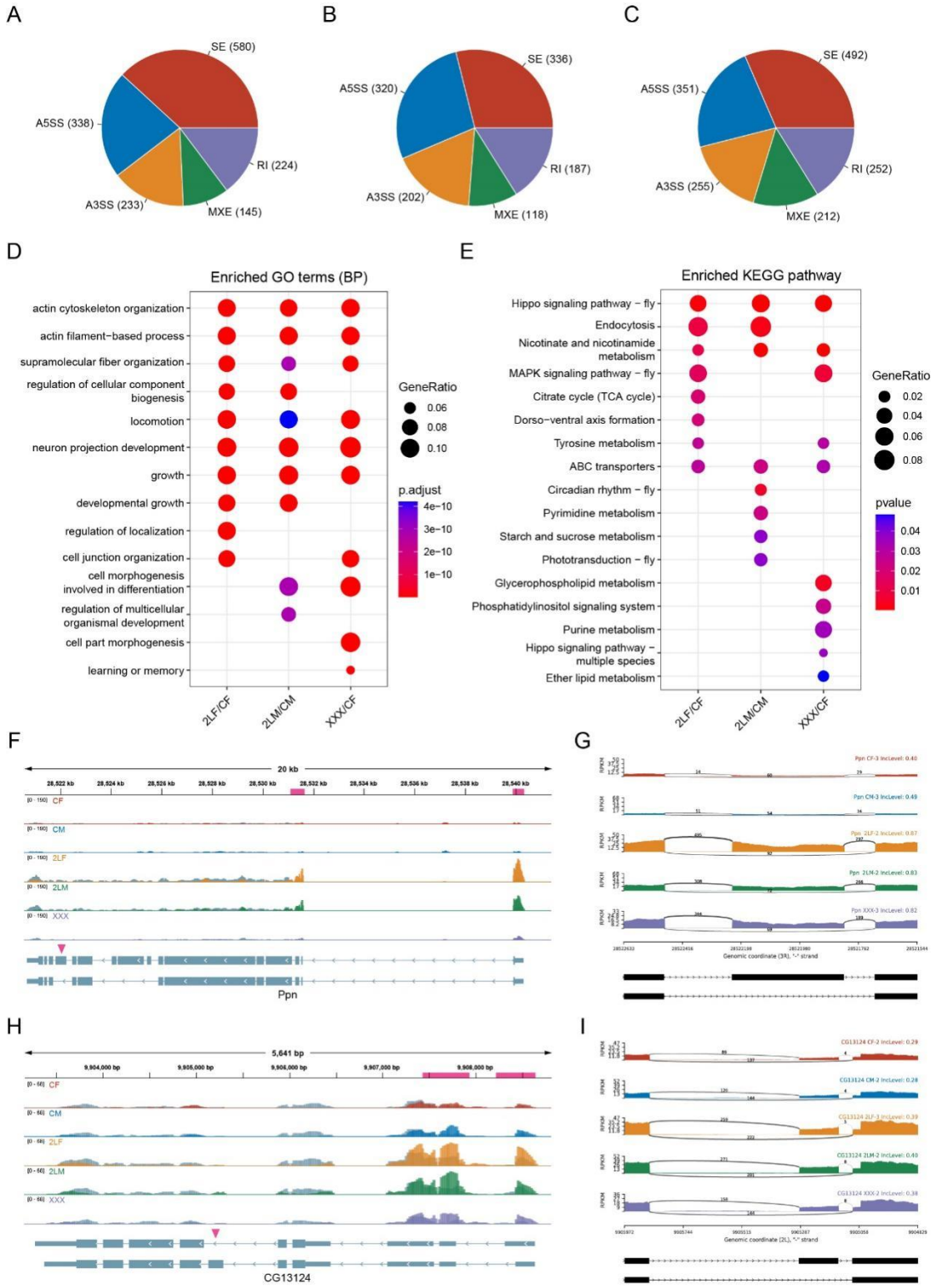

Figure 6—figure supplement 1. Alternative splicing analysis in aneuploidies. (**A**-**C**) Numbers of differential alternative splicing events in trisomy 2L females (**A**), trisomy 2L males (**B**), and metafemales (**C**). SE, skipped exon; A5SS, alternative 5’ splice site; A3SS, alternative 3’ splice site; MXE, mutually exclusive exons; RI, retained intron. (**D**) Functional enrichment analysis of differentially alternatively spliced genes. Top 10 enriched GO terms (Biological Process) with

p-value < 0.05 in each comparison were shown. (**E**) KEGG pathway enrichment analysis of differentially alternatively spliced genes. Top 10 enriched pathways with p-value < 0.05 in each comparison were shown. (**F**,**H**) Genome browser example of *Ppn* (**F**) and *CG13124* (**H**) for indicated MeRIP-seq data. Steelblue color represents input reads, while other colors represent IP reads. Signals were displayed as the mean CPM of two biological replicates. The gene architectures were shown at the bottom (only two representative transcript isoforms were shown). The magenta rectangles at above represent DMPs. The magenta arrowheads indicate the positions of differential alternative splicing. (**G**,**I**) Sashimi plots depicting RNA sequencing reads and exon junction reads at the positions where the differential splicing events occurs on *Ppn* (**G**) and *CG13124* (**I**). The gene models were shown below. One of the biological replicates was chosen for representation. CF, wildtype female control; CM, wildtype male control; 2LF, trisomy 2L female; 2LM, trisomy 2L male; XXX, metafemale; CPM, Counts per million; RPKM, Reads per kilobase per million mapped reads.

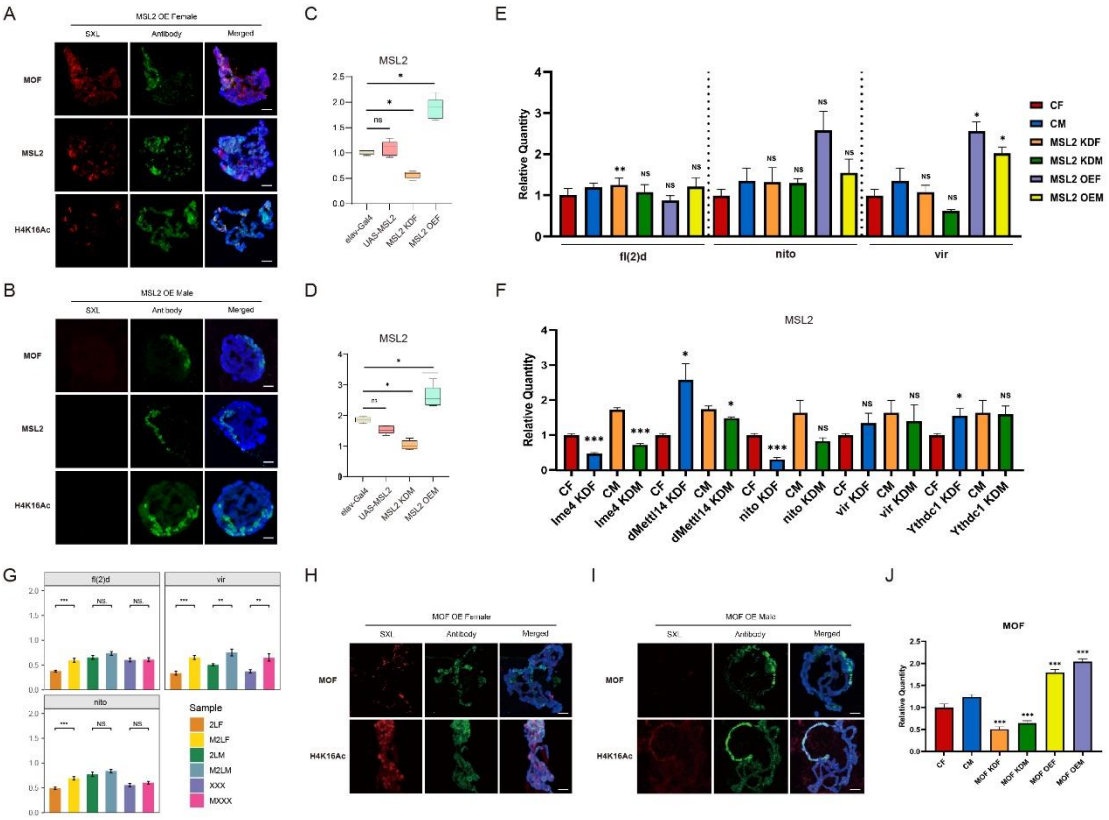

Figure 7—figure supplement 1. The relationships between m^{6}A methylation and MSL complex. (**A**,**C**) Immunofluorescence of polytene chromosomes in MSL2-overexpressed female (**A**) and

male (**C**) larvae. The red channel is the signal from SXL and the green channel is the signal from antibodies of MSL complex components. DNA is stained with DAPI in blue. Scale bars, 10 µm. OE, overexpressed. (**B**,**D**) RT-qPCR analysis of mRNA levels of MSL2 in the heads of MSL2 transgenic female (**B**) and male (**D**) *Drosophila* adults. Student's *t* test *p < 0.05, **p < 0.01, ***p < 0.001. OE, overexpressed. (**E**) RT-qPCR analysis of mRNA levels of m^6A regulators in the heads of MSL2 transgenic *Drosophila*. Student's *t* test *p < 0.05, **p < 0.01, ***p < 0.001. CF, wildtype female control; CM, wildtype male control; OEF, overexpressed female; OEM, overexpressed male; KDF, knockdown female; KDM, knockdown male. (**F**) RT-qPCR analysis of mRNA levels of MSL2 in the heads of m^6A regulators knockdown *Drosophila*. Student's *t* test *p < 0.05, **p < 0.01, ***p < 0.001. CF, wildtype female control; CM, wildtype male control; OEF, overexpressed female; OEM, overexpressed male; KDF, knockdown female; KDM, knockdown male. (**G**) RT-qPCR analysis of mRNA levels of m^6A regulators in the brains of trisomy and MSL2-overexpressed trisomy *Drosophila* larvae. Student's *t* test *p < 0.05, **p < 0.01, ***p < 0.001. 2LF, trisomy 2L female; 2LM, trisomy 2L male; XXX, metafemale; M2LF, MSL2-overexpressed trisomy 2L female; M2LM, MSL2-overexpressed trisomy 2L male; MXXX, MSL2-overexpressed metafemale. (**H**,**I**) Immunofluorescence of polytene chromosomes in MOF-overexpressed female (**H**) and male (**I**) larvae. The red channel is the signal from SXL and the green channel is the signal from MOF or H4K16Ac. DNA is stained with DAPI in blue. Scale bars, 10 µm. OE, overexpressed. (**J**) RT-qPCR analysis of mRNA levels of MOF in the heads of MOF transgenic *Drosophila*. Student's *t* test *p < 0.05, **p < 0.01, ***p < 0.001. CF, wildtype female control; CM, wildtype male control; OEF, overexpressed female; OEM, overexpressed male; KDF, knockdown female; KDM, knockdown male.